2013-07-03

Dynamics and Control of Wrist and Forearm Movements

Allan W. Peaden
Brigham Young University - Provo

Dynamics and Control of Wrist and Forearm Movements

Allan William Peaden

A thesis submitted to the faculty of
Brigham Young University
in partial fulfillment of the requirements for the degree of

Master of Science

Steven K. Charles, Chair
Anton E. Bowden
Mark B. Colton

Department of Mechanical Engineering

Brigham Young University

July 2013

ABSTRACT

Dynamics and Control of Wrist and Forearm Movements

Allan William Peaden
Department of Mechanical Engineering
Master of Science

Wrist and forearm motion is governed both by its dynamics and the control strategies employed by the neuromuscular system to execute goal oriented movement. Two experiments were conducted to increase our understanding of wrist and forearm motion. The first experiment involved 10 healthy subjects executing planned movements to targets involving all three degrees of freedom (DOF) of the wrist and forearm, namely wrist flexion-extension (FE), wrist radial-ulnar deviation, and forearm pronation-supination (PS). A model of wrist and forearm dynamics was developed, and the recorded movements were fed into the model to analyze the movement torques. This resulted in the following key findings: 1) The main impedance torques affecting wrist and forearm movements are stiffness and gravity, with damping and inertial effects contributing roughly 10% of the total torque. 2) There is significant coupling between all degrees of freedom (DOF) of the wrist and forearm, with stiffness effects being the most coupled and inertial effects being the least coupled. 3) Neglecting these interaction torques results in significant error in the prediction of the torque required for wrist and forearm movements, suggesting that the neuromuscular system must account for coupling in movement planning. A second experiment was conducted in which 10 different healthy subjects pointed to targets arranged on a plane in front of the subjects. This pointing task required two DOF, but subjects were allowed to use all three DOF of the wrist and forearm. While subjects could have completed the task with FE and RUD alone, it was found that subjects recruited PS as well. Hypotheses regarding why subjects would recruit PS even though it was not necessary included the minimization of a number of cost functions (work, effort, potential energy, path length) as well as mechanical interaction between the DOF of the wrist and forearm. It was found that the pattern of PS recruitment predicted from the mechanical interaction hypothesis most closely resembled the observed pattern. According to this hypothesis, the neuromuscular system uses a simplified 2 DOF model of the joints most critical to the task (FE and RUD) to plan the task, while leaving the third DOF (PS) uncontrolled. The resulting interaction torques create the observed pattern of PS movement.

Keywords: wrist, forearm, dynamic model, motor control, internal model

ACKNOWLEDGEMENTS

The author is deeply grateful for the time, effort, and tutelage of Dr. Steven K. Charles in this exciting work. Dr. Charles has sacrificed countless hours and many inconveniences to aid the author in all aspects of this research, from conception to completion. The author would also like to express explicit gratitude for Dr. Charles willingness to accept another student into his research group at a time when it was already considered full. Finally, the author would like to thank his friends and family for their support and interest in this research.

TABLE OF CONTENTS

LIST OF TABLES

LIST OF FIGURES

1 INTRODUCTION

1.1 Motivation

Many people today suffer from Repetitive Strain Injuries (RSI) to the wrist, a class of injury that results from repetitive motion, sustained or awkward postures, and general overuse of a joint (van Tulder et al., 2007). Among the general population it is estimated that 11.3% of men and 15.1% of women suffer from such an injury (Walker-Bone et al., 2004). Furthermore, prevalence of RSI has been on the rise in recent decades, particularly among the elderly (Gelfman et al., 2009).

Our ability to understand and treat the causes of RSI to the wrist is limited due to a lack of understanding of several fundamental concepts governing its use and movement. Three areas in which the current body of scientific knowledge falls short include a characterization of the impedance torques acting on the wrist and forearm, the required complexity of the neural internal model of wrist and forearm dynamics, and the control strategy used by the neuromuscular system to plan and control wrist and forearm movements despite kinematic redundancy. The purpose of the present research is to address these issues.

1.1.1 Characterization of Wrist and Forearm Impedance Torques

The joint torques required to execute a movement can be determined by modeling the dynamic behavior of a system of joints. This differs from a static force balance for a body at equilibrium because a dynamic model also includes the effect of velocity and acceleration. In the simplified

static state the only active impedance torques (which the muscle-generated torque must overcome) are torques due to joint stiffness and external forces. Joint stiffness represents the "springiness" of the joint, or the tendency for the joint to return to a neutral position (due to the joint's elastic properties) after being displaced. External forces include gravity and any other externally applied force. However, when a joint is put in motion, dynamic effects become manifest. These include damping effects, which dissipate kinetic energy and are velocity dependent, and inertial effects, which reflect the joint's resistance to change in motion and are either velocity or acceleration dependent.

Our current understanding of the impedance torques that act on the wrist alone (as opposed to the wrist and forearm together) suggests that stiffness and gravitational effects are roughly ten times larger than inertial and damping effects (Charles and Hogan, 2011). However, most natural movements involve the wrist and forearm together, and which impedance effects dominate wrist and forearm movements is currently unknown. Also, that wrist movements are dominated by stiffness effects is in stark contrast to shoulder and elbow movements, which are believed to be dominated by inertial effects. This dichotomy begs the question of whether the forearm rotation (pronation-supination) is more similar to the shoulder and elbow or the wrist.

1.1.2 Complexity of the Neural Internal Model

When executing any voluntary motion the neuromuscular system must first conduct some degree of motor planning, dictating which joints move when, and how much. This planning phase requires some kind of internal model, which has been shown to account for dynamic effects, including velocity and acceleration (Kawato, 1999). However, the required complexity of this internal model remains largely unknown. Specifically, when applied to the wrist and forearm it is

unknown whether all dynamic forces are necessary to the internal model, and whether or not each joint may be considered independently.

1.1.3 Redundancy in the Wrist and Forearm

When considered together the wrist and forearm can be approximated as a universal joint possessing three DOF: flexion-extension (FE), radial-ulnar deviation (RUD), and forearm pronation-supination (PS). Some tasks, such as using the wrist and forearm to point to a target on a plane, require less than three DOF. In the case of pointing, the neuromuscular system could chose to complete this task using only FE and RUD, regardless of the target location–the use of PS in this task is completely optional. The wrist and forearm joints are therefore deemed to be redundant for that task since they are not all necessary.

Prior research has shown that the neuromuscular system makes use of all available DOF in this scenario, and has suggested that there exists a defined plane in RUD-FE-PS space on which all wrist/forearm motion lies (Campolo et al., 2010). Alternative theories for the body's recruitment of all available DOF in this scenario have not yet been examined, and there lacks a clear link between the body's preference in joint use and any physiological explanation.

1.2 Thesis Objective

The purpose of the research presented here is to increase our understanding of the control strategies which govern wrist and forearm movement. The current research contributed to this understanding in the following ways: a characterization of the impedance torques acting on the wrist and forearm, a determination of the needed complexity of an internal model of wrist and forearm dynamics, and an exploration of candidate theories which explain how the neuromuscular handles redundancy involving the wrist and forearm. This understanding is

beneficial for several reasons. A knowledge of which torques have the greatest effect on wrist and forearm movements informs device manufacturers of which type and magnitude of forces most need to be accounted for in human-machine interfaces, orthotics, etc. An understanding of the complexity of the internal wrist and forearm model and a theoretical understanding of how the neuromuscular system handles joint redundancy allows for devices which increase comfort by not interfering with the body's intended paths of joint motion. Conversely, if a device's intended function is to interfere with normal joint motion, such as in therapy, this understanding will allow these devices to be more effective.

Another notable contribution from the present research is a tractable 3-DOF model of wrist and forearm dynamics, incorporating RUD, FE, and PS. This model was used extensively to produce the results of this research, and may find future utility as researchers expand upon this work.

1.3 Thesis Outline

This thesis is organized as follows: Chapter 2 includes a characterization of the impedance torques experienced in normal wrist and forearm movement, and also finds a potential limit for the needed complexity of an internal wrist and forearm model. The last section of Chapter 2 is the derivation of a 3-DOF model of wrist and forearm dynamics, modeled as a universal joint. Chapter 3 focuses on possible solutions to the joint redundancy problem. Experimental results from wrist and forearm movements in an under-constrained scenario are compared to theoretical results based on different control strategies which the neuromuscular system may adapt. Chapter 4 presents the conclusions from this work and provides recommendations for future research.

2 DYNAMICS OF WRIST AND FOREARM ROTATIONS

Prior research indicates that stiffness and gravity dominate the impedance forces in wrist movement, and that a relatively simple internal model of the wrist should be sufficient in many scenarios of small angle movement (Charles and Hogan, 2011). However, these conclusions are limited in that they were only tested for movements in FE and RUD, despite the fact that rotation of the forearm is often used in conjunction with the wrist. Until the present it has been unknown if these same characteristics of pure wrist movement extend to 3 DOF movements involving the forearm. The research presented here addresses the issue, specifically which impedance forces are most significant among RUD FE PS movements, and how complex of a model this more comprehensive system needs be. The contents of this chapter were submitted for publication in the *Journal of Biomechanics*.

2.1 Introduction

Healthy upper limb movements generally involve multiple degrees of freedom gracefully coordinated into a single movement. Despite the apparent ease with which these movements are performed, the underlying dynamics are complex due to coupling (interaction) between the various degrees of freedom (DOF). We recently showed that the two DOF of the wrist, flexion-extension (FE) and radial-ulnar deviation (RUD), are significantly coupled through stiffness (e.g., a wrist rotation in pure FE requires a torque in RUD as well as in FE) (Charles and Hogan, 2011). The control of coordinated wrist rotations must account and compensate for this coupling,

and incomplete compensation has been shown to cause observable path curvature (Charles and Hogan, 2010, 2012). Thus, understanding the coupling between DOF allows us to understand 1) what the neuromuscular system must account and compensate for, 2) why certain behaviors occur (e.g., path curvature), and 3) how loss of compensation (through neuromuscular impairment) or changes in coupling dynamics (e.g., through joint spasticity or tool use) affect behavior.

The purpose of this paper is to characterize the dynamics of forearm rotations and extend our understanding of coupling to rotations involving both wrist and forearm rotations (FE, RUD, and pronation-supination, PS). Many natural movements involve coordination of these three DOF (Aizawa et al., 2010; Anderton and Charles, 2012; van Andel et al., 2008), yet the dynamics of coupled wrist and forearm rotations are unknown. While several computational software packages have been developed to simulate limb dynamics using musculoskeletal parameters (Holzbaur et al., 2005; Lemay and Crago, 1996), here we present a tractable analytical model of wrist and forearm dynamics in terms of joint impedance (stiffness, damping, and inertia) to enable us to compute movement dynamics on a subject-by-subject basis, combining individual subjects' kinematics with measurements of their joint impedance. More specifically, we present a model of wrist and forearm dynamics (involving FE, RUD, and PS) and evaluate these dynamics to answer the following questions:

1. Are forearm rotations (by themselves and combined with simultaneous wrist rotations) dominated by inertial, damping, or stiffness effects?
2. Are the DOF of the wrist (FE and RUD) coupled with the DOF of the forearm (PS)?
3. How complex does a model of wrist and forearm dynamics need to be?

2.2 Methods

2.2.1 Kinematic Data

Subjects

Ten young, healthy, right-handed subjects (5 female and 5 male, ages 19-37) free from neurological and biomechanical injuries to the upper limb were recruited to participate in this experiment. Following procedures approved by Brigham Young University's Institutional Review Board, informed consent was obtained from all subjects.

Experimental setup

Subjects were seated with the upper limb in the parasagittal plane (0° shoulder abduction and approximately 60° elbow flexion). The proximal 14 cm of the forearm rested on a support while the distal forearm, wrist and hand remained unsupported, allowing for unobstructed use of PS, FE, and RUD (Figure 2-1A). Electromagnetic motion tracking sensors (trakSTAR by Ascension Technologies, Burlington, VT) were attached to the distal forearm (approximately 5 cm proximal to the wrist joint center) and atop a handle held by the subject. These sensors recorded orientation at approximately 300Hz with a static accuracy and resolution of 0.5° and 0.1°, respectively. At a combined weight of approximately 75g (5% of the mass of the average hand and forearm), the sensor and handle presented negligible interference to natural movements (see Discussion).

Each subject was calibrated in neutral position, defined as follows. The forearm was in neutral PS when the dorsal aspect of the distal forearm (more specifically the dorsal tubercle of the radius and the dorsal-most aspect of the ulnar head) was in the parasagittal plane. The wrist was in neutral FE and RUD when the long axis of the forearm was parallel to the long axis of the third metacarpal.

Protocol

During the experiment the position of each DOF was communicated to the subject graphically via a computer screen in front of the subject (Figure 2-1B). A cursor on the screen moved horizontally and vertically in proportion to wrist FE and RUD, respectively. A yellow line through the center of this cursor communicated the amount of PS by rotating an equal amount from the vertical (neutral position). FE and RUD targets were represented by a pattern of white circles surrounding the neutral position, while targets in PS were represented by a red line drawn through the cursor. When a target was selected the corresponding circle from the pattern changed color to indicate the required FE and RUD, while the red line assumed the target PS angle. Subjects were required to align the cursor with the target circle and their PS with the target PS (within 2°) before the next target would appear.

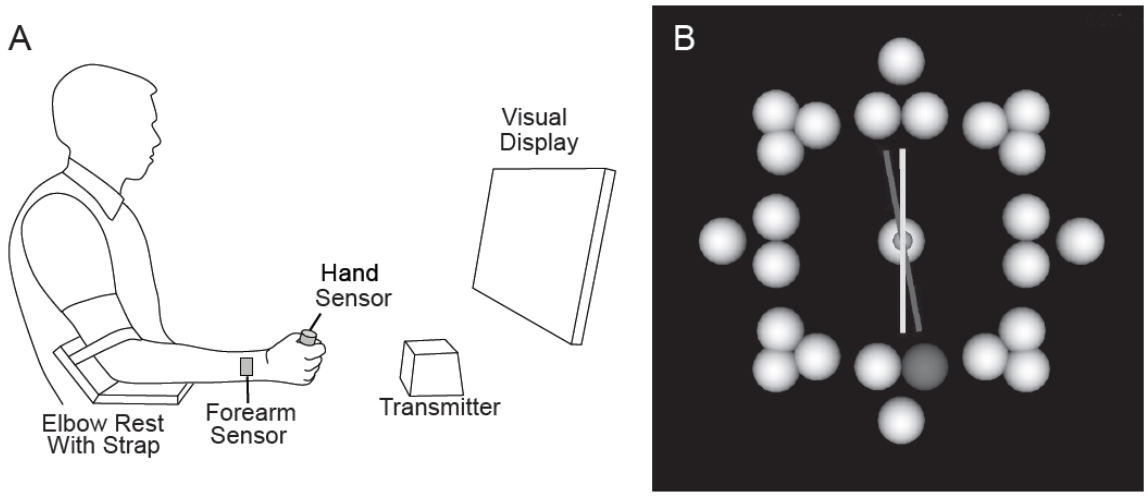

Figure 2-1: Experimental Setup (A) and Visual Display (B). The subject was instructed to move the cursor (visible in the center target) to one of the peripheral targets (a target to the bottom right is visibly highlighted) by use of wrist FE and RUD, while simultaneously aligning the crosshairs (which attached to the cursor) to achieve the desired amount of forearm PS. The darker crosshair is the target PS, while the lighter crosshair represents the subject's current PS.

Targets were selected to require pure PS, FE, and RUD, as well as 2- and 3-way combinations of these DOF. The targets were positioned to require a total angular displacement of 15° in PS, FE, and RUD combined (i.e. rotating the coordinate frame of the hand from neutral to target position required 15° about the common axis). Positive and negative angular displacements were required in each DOF, resulting in a star-like pattern with 26 targets surrounding neutral position (Figure 1B).

Subjects participated in two sessions in which they were instructed to move at a "comfortable speed" or "as fast as possible" (in random order). In each session, subjects made 10 movements to each peripheral target. The data from both sessions were combined for a total of 520 outbound and 520 inbound movements involving combinations of FE, RUD, and PS. Subjects were instructed to move the DOF simultaneously when more than one DOF was required, but were given no further instruction on path shape. As per standard procedure, in each session, the first movement to each target was considered practice and was not included in the analysis.

Data processing

Joint angles were derived from sensor orientation data by inverse kinematics, where PS, FE, and RUD were represented as Euler angles α, β, and γ, respectively (in that order), according to ISB recommendations for global forearm and wrist rotations (Wu et al., 2005). PS, FE, and RUD were positive in pronation, flexion, and ulnar deviation, respectively. The data were low-pass filtered with a fourth order Butterworth filter with a cut-off frequency of 20 Hz) and differentiated to obtain velocity. This process was repeated with the same filter to obtain acceleration, to which the filter was applied one final time. The beginning and end of each

movement were determined based on movement speed, defined as the magnitude of the total angular velocity (see Section 2.5 for derivation):

$$\|\vec{\omega}\| = \sqrt{\dot{\alpha}^2 + \dot{\beta}^2 + \dot{\gamma}^2 + 2\dot{\alpha}\dot{\gamma}\sin\beta} \quad [2\text{-}1]$$

Each movement was then defined to contain all the data points starting at the location of peak speed and extending both before and after this point down to the point at which the speed first descends below 5% of the peak value.

2.2.2 Torque Calculation

The torque in each DOF required to produce the recorded movements were calculated using a 3-DOF model of wrist and forearm dynamics.

Second-order mechanical impedance model of wrist and forearm rotations

The wrist and forearm joints were modeled as a universal joint, with the axes of all three DOF intersecting at the same point. While the RUD axis is believed to be slightly distal to the FE axis, the distance between the axes is small and has been shown to have negligible effect on wrist dynamics (Charles and Hogan, 2011). Likewise, other offsets from the center of rotation are assumed minimal and inconsequential. Inertial, damping, stiffness, and gravitational effects were included for each DOF, resulting in the following equations of motion relating the torque in each DOF to the resulting movement (see Section 2.6 for derivation):

$$\underbrace{\begin{bmatrix} M_\alpha \\ M_\beta \\ M_\gamma \end{bmatrix}}_{\substack{total \\ active \\ torque}} = \underbrace{\begin{bmatrix} A & B & C \\ B & D & E \\ C & E & F \end{bmatrix}\begin{bmatrix} \ddot{\alpha} \\ \ddot{\beta} \\ \ddot{\gamma} \end{bmatrix} + \begin{bmatrix} G \\ H \\ I \end{bmatrix}}_{inertial\ torque} + \underbrace{\begin{bmatrix} B_{\alpha\alpha} & B_{\alpha\beta} & B_{\alpha\gamma} \\ B_{\beta\alpha} & B_{\beta\beta} & B_{\beta\gamma} \\ B_{\gamma\alpha} & B_{\gamma\beta} & B_{\gamma\gamma} \end{bmatrix}\begin{bmatrix} \dot{\alpha} \\ \dot{\beta} \\ \dot{\gamma} \end{bmatrix}}_{damping\ torque} + \underbrace{\begin{bmatrix} K_{\alpha\alpha} & K_{\alpha\beta} & K_{\alpha\gamma} \\ K_{\alpha\beta} & K_{\beta\beta} & K_{\beta\gamma} \\ K_{\alpha\gamma} & K_{\beta\gamma} & K_{\gamma\gamma} \end{bmatrix}\begin{bmatrix} \alpha \\ \beta \\ \gamma \end{bmatrix}}_{stiffness\ torque}$$

$$+ \underbrace{glm\begin{bmatrix} \sin\alpha\sin\gamma - \cos\alpha\cos\gamma\sin\beta \\ -\cos\beta\cos\gamma\sin\alpha \\ \sin\alpha\sin\beta\sin\gamma - \cos\alpha\cos\gamma \end{bmatrix}}_{gravitational\ torque} \qquad [2\text{-}2]$$

Table 2-1: Model parameters

A	$I_{Hx}\sin^2\beta + I_{Hy}\cos^2\beta\cos^2\gamma + I_{Hz}\sin^2\gamma\cos^2\beta + I_{Ay}$
B	$\cos\gamma\cos\beta\sin\gamma\left(I_{Hy} - I_{Hz}\right)$
C	$I_{Hx}\sin\beta$
D	$I_{Hy}\sin^2\gamma + I_{Hz}\cos^2\gamma$
E	0
F	I_{Hx}
G	$I_{Hx}\left[\dot{\beta}\cos\beta\left(\dot{\gamma} + 2\dot{\alpha}\sin\beta\right)\right] + I_{Hy}\left[\cos\beta\cos\gamma\left(\dot{\beta}\dot{\gamma}\cos\gamma - \dot{\alpha}\dot{\beta}\sin\beta\cos\gamma - \dot{\alpha}\dot{\gamma}\cos\beta\sin\gamma\right)\right.$ $\left. - \left(\dot{\beta}\sin\gamma + \dot{\alpha}\cos\beta\cos\gamma\right)\left(\dot{\beta}\sin\beta\cos\gamma + \dot{\gamma}\cos\beta\sin\gamma\right)\right]$ $+ I_{Hz}\left[\cos\beta\sin\gamma\left(\dot{\beta}\dot{\gamma}\sin\gamma + \dot{\alpha}\dot{\gamma}\cos\beta\cos\gamma - \dot{\alpha}\dot{\beta}\sin\beta\sin\gamma\right)\right.$ $\left. + \left(\dot{\beta}\cos\gamma - \dot{\alpha}\cos\beta\sin\gamma\right)\left(\dot{\beta}\sin\beta\sin\gamma - \dot{\gamma}\cos\beta\cos\gamma\right)\right]$
H	$-I_{Hx}\dot{\alpha}\cos\beta\left(\dot{\gamma} + \dot{\alpha}\sin\beta\right)$ $+ I_{Hy}\left[\dot{\alpha}\sin\beta\cos\gamma\left(\dot{\beta}\sin\gamma + \dot{\alpha}\cos\beta\cos\gamma\right)\right.$ $\left. + \dot{\gamma}\cos\gamma\left(2\dot{\beta}\sin\gamma + \dot{\alpha}\cos\beta\cos\gamma\right) - \dot{\alpha}\sin\gamma\left(\dot{\beta}\sin\beta\cos\gamma + \dot{\gamma}\cos\beta\sin\gamma\right)\right]$ $+ I_{Hz}\left[\dot{\alpha}\sin\beta\sin\gamma\left(\dot{\alpha}\cos\beta\sin\gamma - \dot{\beta}\cos\gamma\right)\right.$ $\left. + \dot{\alpha}\cos\gamma\left(\dot{\beta}\sin\beta\sin\gamma - \dot{\gamma}\cos\beta\cos\gamma\right) - \dot{\gamma}\sin\gamma\left(2\dot{\beta}\cos\gamma - \dot{\alpha}\cos\beta\sin\gamma\right)\right]$
I	$I_{Hx}\left(\dot{\alpha}\dot{\beta}\cos\beta\right) + \left(I_{Hy} - I_{Hz}\right)\left(\dot{\beta}\sin\gamma + \dot{\alpha}\cos\beta\cos\gamma\right)\left(\dot{\alpha}\cos\beta\sin\gamma - \dot{\beta}\cos\gamma\right)$

The left-hand side of Equation 2-3 represents active torques (due to muscle contraction), which may depend on displacement and its derivatives (in addition to neural activation) since neural activation affects muscle stiffness and damping. The right-hand side of Equation 2-3 contains the passive inertial, damping, stiffness, and gravitational effects which the active torques must overcome in order to produce movement. The matrix containing elements A through F is the inertia matrix, while G, H, and I contain the centripetal and coriolis terms (Table 2-2). Passive

damping and stiffness (i.e. in the absence of muscle contraction) are represented by the matrices containing damping coefficients (e.g. $B_{\alpha\alpha}$) and stiffness coefficients (e.g. $K_{\alpha\alpha}$), respectively. Parameters g, l, and m represent the gravitational acceleration, distance from the wrist joint to the center mass of the hand, and the mass of the hand, respectively.

Model Parameters

Inertia: Published anthropometric regression equations (de Leva, 1996) were used to estimate the inertia of the hand and forearm, and the mass and center of mass of the hand from measurements of segment lengths from each subject. These equations assume that the body-fixed inertia matrices of the hand and forearm are symmetric (i.e., negligible products of inertia).

Stiffness: The passive stiffness of coupled wrist and forearm rotations was previously measured for each subject by Will Drake in our lab (unpublished data). More specifically, a rehabilitation robot moved each subject's wrist and forearm in combinations of PS, FE, and PS in a quasi-static manner, while it measured the displacement and the torque required to produce that displacement. The 3-DOF stiffness matrix was then estimated from the torque and displacement data by multi-variable linear regression.

Damping: The passive damping associated with coupled wrist and forearm rotations is unknown; however, damping has been measured in flexion-extension to be 0.02-0.03 Nms/rad (Gielen and Houk, 1984). Several studies have found that the stiffness and damping ellipses associated with shoulder and elbow movements are roughly proportional (Dolan et al., 1993; Perreault et al., 2004; Tsuji et al., 1995). Therefore, damping of the wrist and forearm was assumed to be proportional to wrist and forearm stiffness (the constant of proportionality was chosen so that the damping in FE would be 0.03 Nms/rad).

2.2.3 Analysis

Dominant impedance effect

To determine whether wrist and forearm rotations are dominated by inertial, damping, or stiffness effects, we calculated for each movement the average magnitude of the torque vector (in all 3 DOF combined) required to overcome each of these impedance effects as follows:

$$M_j = \frac{1}{T}\int_0^T \left\|\vec{M}_{\alpha,j} + \vec{M}_{\beta,j} + \vec{M}_{\gamma,j}\right\| dt$$
$$= \frac{1}{T}\int_0^T \sqrt{{M_{\alpha,j}}^2 + {M_{\beta,j}}^2 + {M_{\gamma,j}}^2 + 2M_{\alpha,j}M_{\gamma,j}\sin\beta}\, dt \qquad [2\text{-}3]$$

where *j* represents the impedance element (either inertia, damping, stiffness) or gravity (we did not consider gravity as an intrinsic element but included it in the analysis—see Discussion), and T is the duration of the movement. We tested for differences in M_j between impedance elements by 2-way ANOVA with impedance element and subject as fixed and random factors, respectively.

Interaction between degrees of freedom

In general, the DOF of a multi-DOF system are coupled, meaning that the torque in a DOF depends not only on movement in that DOF but also on movement in other DOF. In other words, the total torque in a DOF can be divided into a main torque (the torque in that DOF due to movement in that DOF) and an interaction torque (the torque in that DOF due to movement in other DOF). To quantify the amount of coupling between DOF, we computed for each movement the ratio of the average magnitude of the interaction torque vector to the average magnitude of the main torque vector:

$$R = \frac{\frac{1}{T}\int_0^T \left\|\vec{M}_{\alpha,IT} + \vec{M}_{\beta,IT} + \vec{M}_{\gamma,IT}\right\| dt}{\frac{1}{T}\int_0^T \left\|\vec{M}_{\alpha,MT} + \vec{M}_{\beta,MT} + \vec{M}_{\gamma,MT}\right\| dt} \quad [2\text{-}4]$$

where IT and MT stand for interaction torque and main torque, respectively (the vector sum in the numerator and denominator was calculated as in Equation 2-3. According to this definition, a larger value of R indicates greater coupling between DOF. Main torques were obtained from Equation 2-3 by including only the diagonal elements of each matrix, while interaction torques were obtained by only including the off-diagonal elements (G, H, and I were included in the inertial interaction torque). Gravitational effects were not included in this portion of the analysis. We also computed this ratio separately for inertia, damping, and stiffness:

$$R_j = \frac{\frac{1}{T}\int_0^T \left\|\vec{M}_{\alpha,IT,j} + \vec{M}_{\beta,IT,j} + \vec{M}_{\gamma,IT,j}\right\| dt}{\frac{1}{T}\int_0^T \left\|\vec{M}_{\alpha,MT,j} + \vec{M}_{\beta,MT,j} + \vec{M}_{\gamma,MT,j}\right\| dt} \quad [2\text{-}5]$$

where j represents the impedance element (inertia, damping, or stiffness). We tested for differences in R_j between impedance element by 2-way ANOVA with impedance element and subject as fixed and random factors, respectively.

Model complexity

To determine how complex a model of wrist and forearm dynamics needs to be, we tested the accuracy of a series of simplifying approximations of Equation 2-3. In the first approximation, centripetal and coriolis terms (G, H, and I in Eq.) were neglected; the second simplification involved linearizing the first approximation about the neutral position. The third and final approximation neglected coupling between DOF (the off-diagonal terms of the impedance matrices). The error associated with each approximation was computed at each instant as $\left\|\vec{M} - \vec{M}'\right\|$, the magnitude of the difference between the complete torque vector ($\vec{M} = \vec{M}_\alpha + \vec{M}_\beta + \vec{M}_\gamma$) and the approximate torque vector ($\vec{M}' = \vec{M'}_\alpha + \vec{M'}_\beta + \vec{M'}_\gamma$). The

magnitude of the mean and maximum error values for each movement were then computed and expressed as a percentage of the magnitude of the maximum complete torque of that movement.

2.3 Results

2.3.1 Dominant Impedance Effect

Most of the wrist and forearm torque required to make 15° forearm or simultaneous wrist and forearm rotations is used to overcome gravity and passive stiffness (Figure 2-2A-B). In comparison, the torques required to overcome inertial and damping effects are one order of magnitude smaller. Because they depend on acceleration and/or velocity, inertial and damping torques increase with speed (while gravity and stiffness torques do not), but even at the fastest speeds (in movements with durations less than 250ms) they only account for 15% and 25% of the total torque, respectively. While the four torque components can clearly be divided into two groups based on magnitude (gravitational and stiffness effects vs. damping and inertial effects; Figure 2-2A-B), there was a statistically significant difference between all four elements: $M_{grav} > M_{stiff} > M_{damp} > M_{inertia}$ ($p<0.0001$). This same ordering is true for movements to targets involving only PS ($p<0.0001$;Figure 2-2 C-D).

We also compared torque components between DOF and found that the size of inertial and gravitational effects remained relatively constant across DOF, while stiffness and damping effects were more pronounced in pure RUD than in pure FE or PS because stiffness and damping are significantly greater in RUD than in FE and PS (Figure 2-3) (according to the measurements of 3-DOF stiffness performed by Will Drake in our lab; unpublished data). Coupled movements lie between these extremes.

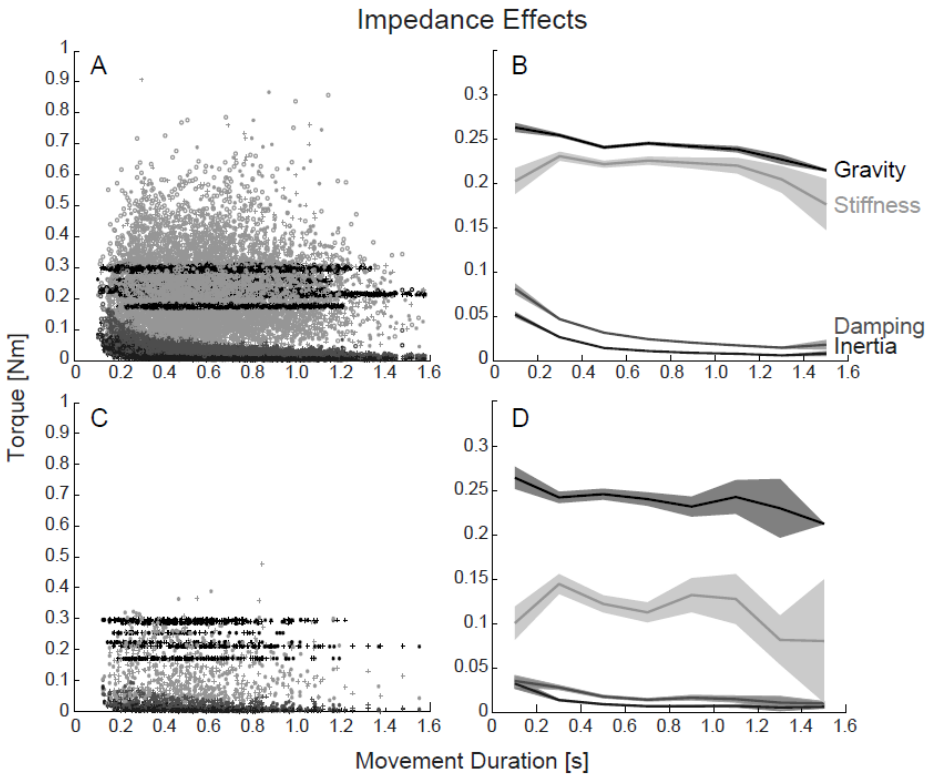

Figure 2-2: The contribution of inertia, damping, stiffness, and gravity (color code in plot B) to movements involving PS, FE, and RUD (plots A and B) and only PS (plots C and D). Individual movements are represented in plots A and C (+, *, and ○ represent movements involving pronation, supination, or neither, respectively; C only contains movements involving pronation or supination). Average effects are shown in plots B and D, with mean effects (thick line) and 95% confidence interval of the mean (shaded area) for the data in figures (A) and (C), respectively.

2.3.2 Interaction Between Degrees of Freedom

The ratio of interaction torque to main torque was 18 ± 13% and relatively constant across movement durations (Figure 2-4). Considering inertia, damping, and stiffness separately, the ratio of the interaction torque to main torque was 8.9 ± 4.1% (mean ± SD) for inertia, 18 ± 11% for damping, and 18 ± 12% for stiffness. While these ratios are of the same order of magnitude, there were statistically significant differences between them: $R_{stiff} > R_{damp} > R_{inertia}$ ($p<0.001$).

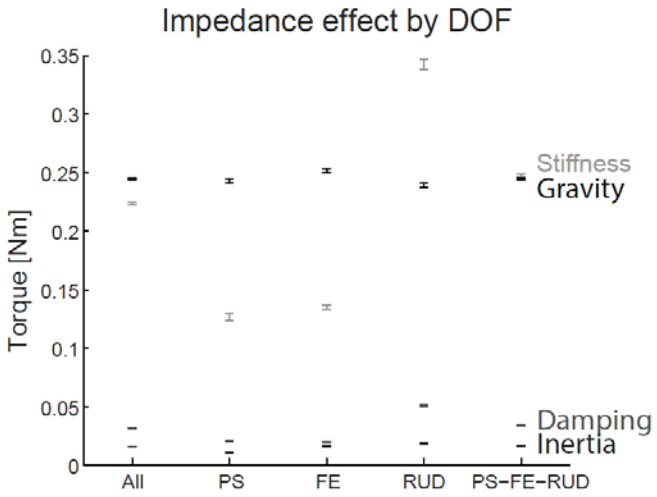

Figure 2-3: Mean impedance effect (color code to the right) grouped by DOF. The category *All* includes all movements, the categories *PS*, *FE*, and *RUD* contain movements to targets involving only a single DOF, and the category *PS-FE-RUD* represents movements requiring simultaneous motion in all three DOF. In all categories, gravity effects are greater than damping effects, which are greater than inertial effects, while the relative size of gravity and stiffness effects vary by category (because stiffness is significantly larger in RUD than in the other DOF). The error bars represent 1 standard error.

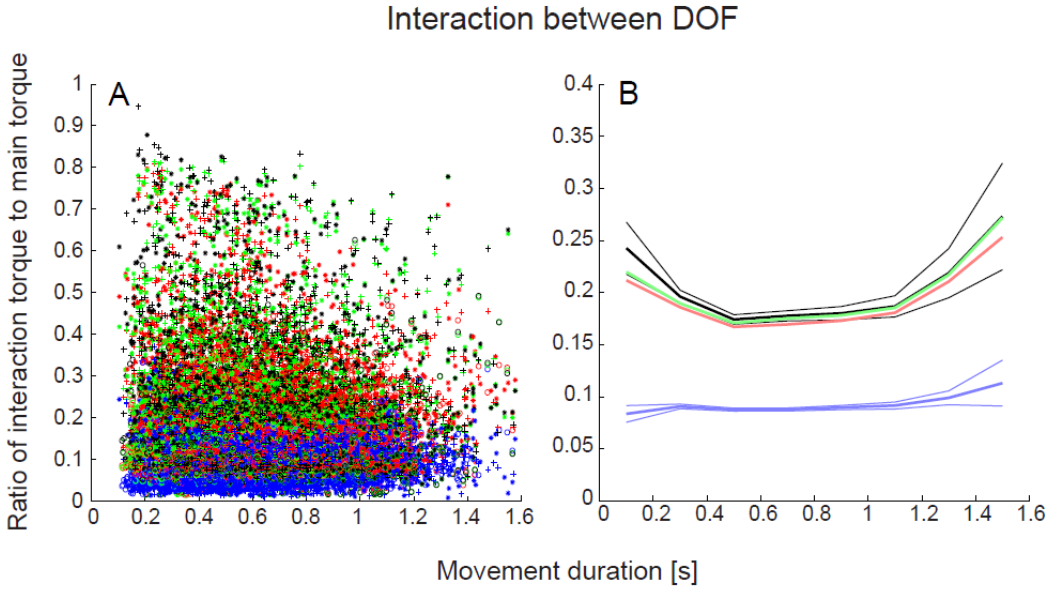

Figure 2-4: Ratio of interaction torque to main torque for inertia (blue), damping (red), and stiffness (green) for individual movements (A) and averaged over all movements (B) (note the difference in scale between vertical axes). The meaning of the marker symbols in A is the same as in Figure 2-2. The error bars in B represent the 95% confidence interval of the mean.

2.3.3 Model Complexity

Some of the torques in Equation 2-3 contribute little to the total torque and can be neglected with little loss in accuracy (Figure 2-5), allowing the use of the following approximate models under certain conditions.

Approximation 1

Neglecting the velocity-dependent inertial interaction torques (the centripetal and coriolis torques) by setting $G = H = I = 0$ produced mean and maximum error values of only 0.08 and 0.54%, respectively.

Approximation 2

Approximation 1 was further simplified by linearizing the torques about neutral wrist and forearm position ($\alpha = \beta = \gamma = 0$), resulting in the following set of linear equations:

$$\begin{bmatrix} M_\alpha \\ M_\beta \\ M_\gamma \end{bmatrix} = \begin{bmatrix} I_{Hy} + I_{Ay} & \gamma(I_{Hy} - I_{Hz}) & I_{Hx} \cdot \beta \\ \gamma(I_{Hy} - I_{Hz}) & I_{Hz} & 0 \\ I_{Hx} \cdot \beta & 0 & I_{Hx} \end{bmatrix} \begin{bmatrix} \ddot{\alpha} \\ \ddot{\beta} \\ \ddot{\gamma} \end{bmatrix} + \begin{bmatrix} B_{\alpha\alpha} & B_{\alpha\beta} & B_{\alpha\gamma} \\ B_{\beta\alpha} & B_{\beta\beta} & B_{\beta\gamma} \\ B_{\gamma\alpha} & B_{\gamma\beta} & B_{\gamma\gamma} \end{bmatrix} \begin{bmatrix} \dot{\alpha} \\ \dot{\beta} \\ \dot{\gamma} \end{bmatrix}$$
$$+ \begin{bmatrix} K_{\alpha\alpha} & K_{\alpha\beta} & K_{\alpha\gamma} \\ K_{\alpha\beta} & K_{\beta\beta} & K_{\beta\gamma} \\ K_{\alpha\gamma} & K_{\beta\gamma} & K_{\gamma\gamma} \end{bmatrix} \begin{bmatrix} \alpha \\ \beta \\ \gamma \end{bmatrix} + glm \begin{bmatrix} -\beta \\ -\alpha \\ -1 \end{bmatrix} \quad [2\text{-}6]$$

This small-angle approximation resulted in mean and maximum error values of only 0.83% and 1.9%, respectively.

Approximation 3

In the third approximation, the torque in each DOF was uncoupled from movement in other DOF by neglecting off-diagonal parameters, resulting in:

$$M_\alpha = \ddot{\alpha}\left(I_{Hy} + I_{Ay}\right) + \dot{\alpha}B_{\alpha\alpha} + \alpha K_{\alpha\alpha}$$

$$M_\beta = \ddot{\beta}I_{Hz} + \dot{\beta}B_{\beta\beta} + \beta K_{\beta\beta} \qquad [2\text{-}7]$$

$$M_\gamma = \ddot{\gamma}I_{Hx} + \dot{\gamma}B_{\gamma\gamma} + \gamma K_{\gamma\gamma} - glm$$

This final approximation caused a significantly larger values of 9.7% and 17% in the mean and maximum errors, respectively.

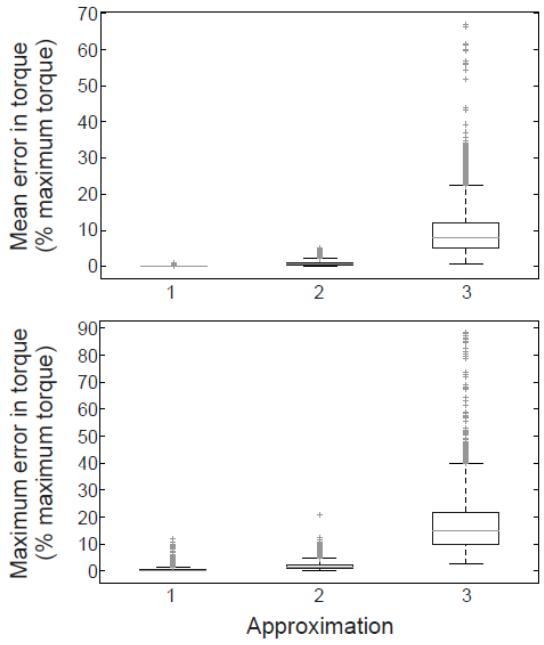

Figure 2-5: Box plots of the mean and maximum error in torque (averaged across all subjects) due to the following approximations: 1) Omitting the velocity-dependent inertial terms, 2) linearizing about the neutral position, and 3) decoupling the DOF.

2.4 Discussion

Coordinated movement requires joint torques to account and compensate for the mechanical impedance (inertial, damping, stiffness) and gravitational effects in each DOF. Much of the upper limb motor control research over the past several decades has focused on how the neuromuscular system controls the inertial dynamics of reaching (shoulder and elbow) movements, in particular the significant and complex inertial interaction torques that couple the

shoulder and elbow joints (Hollerbach and Flash, 1982). In contrast, we have recently shown that wrist rotations are dominated by stiffness, not inertial effects, that the two DOF of the wrist are significantly coupled by stiffness and damping (but not inertia), and that a simple, linear model of wrist dynamics may be sufficient for planning and controlling wrist rotations (Charles and Hogan, 2011). The contrast between shoulder-elbow dynamics and wrist dynamics raises the question of whether the dynamics of the intermediate DOF (forearm pronation-supination, PS) are more similar to those of its proximal neighbors or its distal neighbor.

Here we show that the dynamics of forearm rotations are 1) similar to those of wrist rotations in that stiffness effects dominate over inertial effects and that dynamics are well-approximated by simple, linear equations of motion, and 2) intermediate between wrist and shoulder-elbow dynamics in that combined wrist and forearm rotations are coupled by stiffness, damping, and inertial effects.

2.4.1 Dominant Impedance Effect

Our results indicate that forearm rotations are similar to wrist rotations in that stiffness effects heavily dominate over inertial and damping effects. The same is true for movements combining wrist and forearm rotations. While we included gravitational effects in the analysis, we did not consider gravity to be an intrinsic impedance effect because the magnitude of its effect depends on the orientation of the forearm with respect to an external reference frame. In this study, the forearm was in the horizontal plane, maximizing the gravitational torque of the hand about the wrist joint. Therefore, the magnitude of the gravitational effects presented in this paper would decrease as the long axis of the forearm is rotated from horizontal to vertical. The relatively small magnitude of inertial effects supports the claim that the mass of the handle and sensors

would have negligible impact on the results. Increasing the wrist and forearm mass by 5% would not alter any of the key findings presented here.

2.4.2 Interaction Between Degrees of Freedom

Although the coupling between the three DOF of the wrist and forearm is smaller than the main effects (by a factor of five), it is not negligible, as demonstrated by the relatively large error associated with the removal of coupling in Approximation 3. The amount of coupling in inertia, damping, and stiffness is of the same order of magnitude (9%, 19%, and 19%, respectively). This result differs dramatically from prior studies involving only the wrist (Charles and Hogan, 2011), where inertial interaction torques were found to be negligible compared to damping and stiffness interaction torques (0.3% for inertia vs. approximately 13% for stiffness and damping). The reason why the ratio of interaction to main torques is larger in the current study (for stiffness and damping as well as inertia) is because we considered interaction across more DOF than in the previous study (e.g., we included the torque in PS due to movement in FE and/or RUD, which was not included in the previous study). The reason why the increase in inertial coupling from the previous to the current study is much greater than the increase in damping and stiffness coupling is because the inertial coupling between FE and RUD is very weak (because the inertia in these two DOF is very similar), whereas the inertial coupling of FE and RUD with PS is of the same order of magnitude as stiffness and damping coupling.

2.4.3 Model Complexity

Inertial interaction torques can be classified as acceleration-dependent (B, C, and E in Equation 2-3) and velocity-dependent terms (G, H, and I, which contain the centripetal and coriolis terms).

While the inertial interaction torques as a whole are not negligible (9% of total torque), the velocity-dependent inertial interaction torques are (the mean error from Approximation 1 was 0.08%). As these terms are the most complex terms in the equations of motion, neglecting these terms (Approximation 1) greatly simplifies the equations of motion.

Linearizing the equations of motion (which neglects other terms in addition to G, H, and I) produces a larger but still negligible error (mean error of 0.86%). While this approximation is a substantial improvement in simplicity, it is only valid for modestly sized rotations (displacements on the order of ±15°, as in this study).

In contrast, appreciable error (mean 9.7%) was accumulated when attempting to decouple the system. This fact further solidifies the importance of interaction torques in wrist and forearm rotations, and helps define a possible limit as to the needed complexity of an internal model of the wrist and forearm. In other words, this finding suggests that the neuromuscular system could control modestly sized wrist and forearm rotations by the simple, linear equations of motion in Approximation 2.

2.4.4 Model Robustness

Care was taken to minimize errors in modeling the torques required for wrist and forearm rotations. The stiffness values used in this study were measured on each subject and are similar to previous measurements of wrist and forearm stiffness. Inertial values were derived from measurements of segment lengths measured on each subject. More importantly, the main conclusions of this study are relatively insensitive to reasonable errors in model parameters because the differences between variables are large. For example, our results show that stiffness torques are one order of magnitude greater than inertial and damping torques. To reverse this

dominance of stiffness would require unreasonably large errors in our model parameters. Finally, the main conclusions of this study (that stiffness dominates impedance effects and that coupling is non-negligible) were found to be true for individual subjects as well as all subjects combined.

2.5 Derivation of Wrist and Forearm Movements Angular Velocity Magnitude

The magnitude of the angular velocity of wrist and forearm movements can be determined using kinematics and individual joint angles and velocities. Assuming that all available DOF (RUD, FE, and PS) having intersecting axis (forming a universal joint) then the angular velocity of the final position is:

$$\omega = \dot{\gamma}\hat{\imath}'' + \dot{\alpha}\hat{\jmath} + \dot{\beta}\hat{k}' \qquad [2\text{-}8]$$

where $\hat{\imath}''$ is the coordinate frame of the hand and forearm after displacements in PS and FE, $\hat{\jmath}$ is the stationary coordinate frame, and $\hat{k}'$ is the coordinate frame of the hand and forearm after a displacement in PS (Figure 2-6). The following rotation matrices map a point into the rotating coordinate frame defined by the Euler angles α, β and γ, representing PS, FE, and RUD, respectively:

$$R_\gamma = \begin{bmatrix} 1 & 0 & 0 \\ 0 & \cos\gamma & \sin\gamma \\ 0 & -\sin\gamma & \cos\gamma \end{bmatrix}, R_\beta = \begin{bmatrix} \cos\beta & \sin\beta & 0 \\ -\sin\beta & \cos\beta & 0 \\ 0 & 0 & 1 \end{bmatrix}, R_\alpha = \begin{bmatrix} \cos\alpha & 0 & -\sin\alpha \\ 0 & 1 & 0 \\ \sin\alpha & 0 & \cos\alpha \end{bmatrix} \qquad [2\text{-}9]$$

Applying the above rotation matrices to bring ω into a stationary frame yield:

$$\omega = [R_\alpha]^T \left[R_\beta\right]^T \dot{\gamma}\hat{\imath} + \dot{\alpha}\hat{\jmath} + [R_\alpha]^T \dot{\beta}\hat{k} \qquad [2\text{-}10]$$

$$\omega = \hat{\jmath}\dot{\alpha} + \left(\sin\alpha\,\hat{\imath} + \cos\alpha\,\hat{k}\right)\dot{\beta} + \left(\cos\alpha\cos\beta\,\hat{\imath} + \sin\beta\,\hat{\jmath} - \sin\alpha\cos\beta\,\hat{k}\right)\dot{\gamma} \qquad [2\text{-}11]$$

Rearranged:

$$\omega = \left(\dot{\gamma}\cos\alpha\cos\beta + \dot{\beta}\sin\alpha\right)\hat{\imath} + (\dot{\alpha} + \dot{\gamma}\sin\beta)\hat{\jmath} + \left(\dot{\beta}\cos\alpha - \dot{\gamma}\sin\gamma\cos\beta\right)\hat{k} \qquad [2\text{-}12]$$

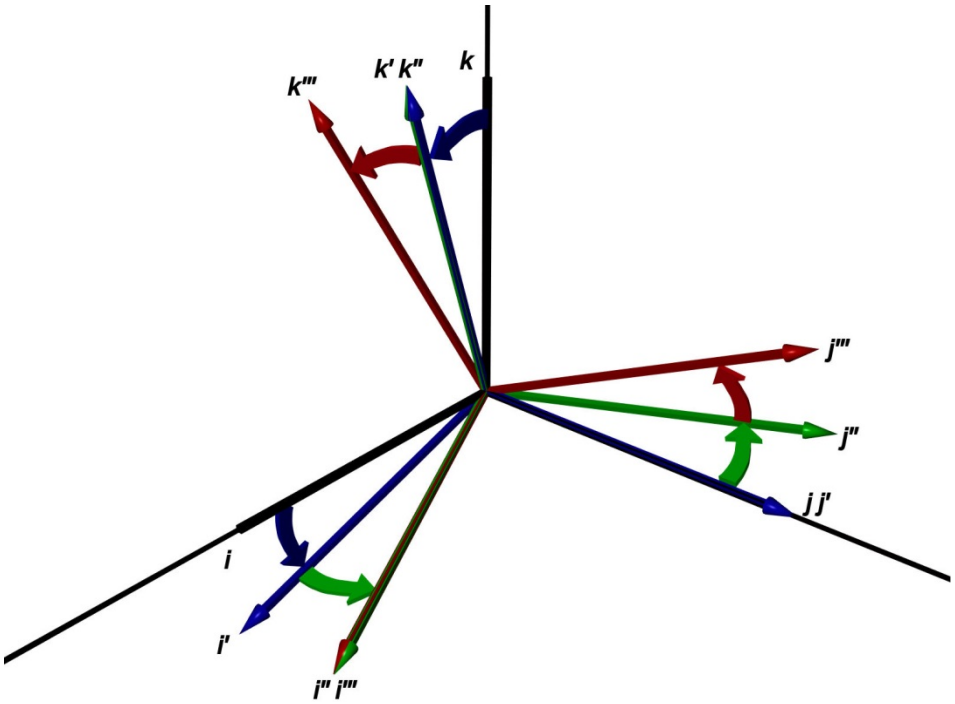

Figure 2-6: Coordinate frame for angular velocity derivation

The magnitude is found by computing

$$\|\omega\| = \sqrt{\omega \cdot \omega} \qquad [2\text{-}13]$$

Which, when expanded, is:

$$\begin{aligned}\omega = \Big(& \left(\dot{\gamma}^2 \cos^2\alpha \cos^2\beta + 2\,\dot{\gamma}\dot{\beta}\sin\alpha\cos\alpha\cos\beta + \dot{\beta}^2\sin^2\alpha\right) \\ & + \left(\dot{\alpha}^2 + 2\dot{\alpha}\dot{\gamma}\sin\beta + \dot{\gamma}^2\sin^2\beta\right) \\ & + \left(\dot{\beta}^2\cos^2\alpha - 2\,\dot{\gamma}\dot{\beta}\sin\alpha\cos\alpha\cos\beta + \dot{\gamma}^2\sin^2\alpha\cos^2\beta\right)\Big)^{1/2}\end{aligned} \qquad [2\text{-}14]$$

Simplifying the above equation and regrouping:

$$\begin{aligned}\omega = \Big(& \left(\dot{\alpha}^2 + 2\dot{\alpha}\dot{\gamma}\sin\beta + \dot{\beta}^2(\cos^2\alpha + \sin^2\alpha)\right. \\ & \left. + \dot{\gamma}^2(\cos^2\alpha\cos^2\beta + \sin^2\beta + \sin^2\alpha\cos^2\beta)\right)^{1/2}\end{aligned} \qquad [2\text{-}15]$$

Removing trigonometric identities results in:

$$\|\vec{\omega}\| = \sqrt{\dot{\alpha}^2 + \dot{\beta}^2 + \dot{\gamma}^2 + 2\dot{\alpha}\dot{\gamma}\sin\beta} \quad [2\text{-}16]$$

2.6 Derivation of 3-DOF Model of Wrist and Forearm Dynamics

The wrist and forearm were modeled as a universal joint with the following assumptions:

- The axis of all three degrees of freedom (DOF) intersect at a common point (the center of the wrist joint)
- Stiffness and damping are linear in all DOF
- The center of mass of the forearm lies on the axis of rotation of the forearm

We derived the equations of motion using Lagrange's Equation:

$$Q_k = \frac{d}{dt}\left(\frac{\partial L}{\partial \dot{q}_k}\right) - \frac{\partial L}{\partial q_k} \quad [2\text{-}17]$$

Variables q_k and $Q_k$represent the k^{th} generalized coordinate and force, respectively, which were defined as follows: α, β, and γ are Euler angles (in that order) representing angular displacement in forearm pronation-supination (PS), wrist flexion-extension (FE), and wrist radial-ulnar deviation (RUD), respectively (with pronation, flexion, and ulnar deviation defined as positive). Torques M_α, M_β, and M_γ represent the total active torques (due to muscle contraction, which includes active stiffness and damping effects) about the axes associated with α, β, and γ.

The generalized forces were determined by the method of virtual work:

$$\delta W^{nc} = Q_\alpha \delta\alpha + Q_\beta \delta\beta + Q_\gamma \delta\gamma \quad [2\text{-}18]$$

$$\delta W^{nc} = M_\alpha \delta\alpha + M_\beta \delta\beta + M_\gamma \delta\gamma - \begin{bmatrix} B_{\alpha\alpha} & B_{\alpha\beta} & B_{\alpha\gamma} \\ B_{\beta\alpha} & B_{\beta\beta} & B_{\beta\gamma} \\ B_{\gamma\alpha} & B_{\gamma\beta} & B_{\gamma\gamma} \end{bmatrix} \begin{bmatrix} \dot{\alpha} \\ \dot{\beta} \\ \dot{\gamma} \end{bmatrix} \cdot \begin{bmatrix} \delta\alpha \\ \delta\beta \\ \delta\gamma \end{bmatrix} \quad [2\text{-}19]$$

where B_{ij} represents the passive damping (i.e. in the absence of muscle contraction) in i due to movement in j (for $i, j = \alpha, \beta, or\ \gamma$). Setting these expressions equal to each other results in the generalized forces:

$$Q_\alpha = M_\alpha - B_{\alpha\alpha}\dot{\alpha} - B_{\alpha\beta}\dot{\beta} - B_{\alpha\gamma}\dot{\gamma}$$

$$Q_\beta = M_\beta - B_{\beta\alpha}\dot{\alpha} - B_{\beta\beta}\dot{\beta} - B_{\beta\gamma}\dot{\gamma} \quad [2\text{-}20]$$

$$Q_\gamma = M_\gamma - B_{\gamma\alpha}\dot{\alpha} - B_{\gamma\beta}\dot{\beta} - B_{\gamma\gamma}\dot{\gamma}$$

The total kinetic energy of the system can be described by:

$$T = \frac{1}{2}m_h\dot{r}_h \cdot \dot{r}_h + \frac{1}{2}[\omega_h]^T[I_h][\omega_h] + \frac{1}{2}[\omega_a]^T[I_A][\omega_a] \quad [2\text{-}21]$$

where

m_h	is the total mass of the hand
r_h	is the vector from the wrist joint center to the center of mass (COM) of the hand
ω_h	is the angular velocity vector of the hand
I_h	is the inertia matrix of the hand about body-fixed axes centered in the hand COM
ω_a	is the angular velocity vector of the forearm
I_A	is the inertia matrix of the forearm about body-fixed axes centered in the forearm COM
T	is the transpose operation

Assuming symmetry, the inertia matrices were defined as:

$$I_h = \begin{bmatrix} I_{hx} & 0 & 0 \\ 0 & I_{hy} & 0 \\ 0 & 0 & I_{hz} \end{bmatrix} \quad [2\text{-}22]$$

$$and \quad I_A = \begin{bmatrix} I_{Ax} & 0 & 0 \\ 0 & I_{Ay} & 0 \\ 0 & 0 & I_{Az} \end{bmatrix} \quad [2\text{-}23]$$

The universal joint forces the following relationships:

$$r_h = -l\hat{j}''' \quad [2\text{-}24]$$

$$\omega_h = \dot{\gamma}\hat{\imath}'' + \dot{\alpha}\hat{\jmath} + \dot{\beta}\hat{k}' \quad [2\text{-}25]$$

$$\omega_\alpha = 0\hat{\imath} + \dot{\alpha}\hat{\jmath} + 0\hat{k} \quad [2\text{-}26]$$

where l represents the distance from the wrist joint center to the COM of the hand, and $\hat{\imath}$, $\hat{\jmath}$, and $\hat{k}$ represent unit vectors along the axes associated with α, β, and γ, respectively. The number of primes represents each successive Euler angle rotation (e.g., $\hat{\imath}$ represents neutral orientation and $\hat{\imath}'$, $\hat{\imath}''$, and $\hat{\imath}'''$ represent orientation after rotation by α, β, and γ, respectively). The rotation matrices relating neutral orientation (the $\hat{\imath}\hat{\jmath}\hat{k}$ frame) to the actual orientation (the $\hat{\imath}'''\hat{\jmath}'''\hat{k}'''$ frame) are:

$$R_\gamma = \begin{bmatrix} 1 & 0 & 0 \\ 0 & \cos\gamma & \sin\gamma \\ 0 & -\sin\gamma & \cos\gamma \end{bmatrix}, R_\beta = \begin{bmatrix} \cos\beta & \sin\beta & 0 \\ -\sin\beta & \cos\beta & 0 \\ 0 & 0 & 1 \end{bmatrix}, R_\alpha = \begin{bmatrix} \cos\alpha & 0 & -\sin\alpha \\ 0 & 1 & 0 \\ \sin\alpha & 0 & \cos\alpha \end{bmatrix} \quad \begin{matrix} [2\text{-}27] \\ [2\text{-}28] \\ [2\text{-}29] \end{matrix}$$

Therefore, ω_h can be re-written as

$$\omega_h = \dot{\gamma}\hat{\imath}''' + [R_\gamma][R_\beta]\begin{bmatrix} 0 \\ \dot{\alpha} \\ 0 \end{bmatrix}\hat{\jmath}''' + [R_\gamma]\begin{bmatrix} 0 \\ 0 \\ \dot{\beta} \end{bmatrix}\hat{k}''' \quad [2\text{-}28]$$

$$\omega_h = (\dot{\gamma} + \dot{\alpha}\sin\beta)\hat{\imath}''' + \left(\dot{\beta}\sin\gamma + \dot{\alpha}\cos\beta\cos\gamma\right)\hat{\jmath}''' + \left(\dot{\beta}\cos\gamma - \dot{\alpha}\cos\beta\sin\gamma\right)\hat{k}''' \quad [2\text{-}29]$$

Determining $\dot{r}_h$ requires the derivative of $\hat{\jmath}$ in the $\hat{\imath}'''\hat{\jmath}'''\hat{k}'''$ frame, which can be derived using the formula $\dot{\hat{e}} = \frac{\partial e}{\partial t} + \vec{\omega}_{total} \times \hat{e}$ (where $\hat{e}$ represents a generic vector):

$$\dot{\hat{\jmath}}''' = \frac{\partial \hat{\jmath}'''}{\partial t} + \omega_h \times \begin{bmatrix} 0 \\ 1 \\ 0 \end{bmatrix} = \left(\dot{\alpha}\cos\beta\sin\gamma - \dot{\beta}\cos\gamma\right)\hat{\imath}''' + (0)\hat{\jmath}''' + (\dot{\gamma} + \dot{\alpha}\sin\beta)\hat{k}''' \quad [2\text{-}30]$$

Therefore, $\dot{r}_h$can be re-written

$$\dot{r}_h = l\left(\dot{\beta}\cos\dot{\gamma} - \alpha\cos\beta\sin\gamma\right)\hat{\imath}''' - l(\dot{\gamma} + \dot{\alpha}\sin\beta)\hat{k}''' \quad [2\text{-}31]$$

Inserting into Equation 2-21 results in the following expression for the kinetic energy:

$$\begin{aligned} T = {} & \frac{1}{2}ml^2(\dot{\gamma} + \dot{\alpha}\sin\beta)^2\left(\dot{\beta}\cos\gamma - \dot{\alpha}\cos\beta\sin\gamma\right)^2 + \frac{1}{2}I_{hx}(\dot{\gamma} + \dot{\alpha}\sin\beta)^2 \\ & + \frac{1}{2}I_{hy}\left(\dot{\beta}\sin\gamma + \dot{\alpha}\cos\beta\cos\gamma\right)^2 + \frac{1}{2}I_{hz}\left(\dot{\beta}\cos\gamma - \dot{\alpha}\cos\beta\sin\gamma\right)^2 \\ & + \frac{1}{2}I_{Ay}\dot{\alpha}^2 \end{aligned} \quad [2\text{-}32]$$

The potential energy is a combination of the potential energy due to gravitational and stiffness effects:

$$V = \frac{1}{2}[\alpha \quad \beta \quad \gamma]\begin{bmatrix} K_{\alpha\alpha} & K_{\alpha\beta} & K_{\alpha\gamma} \\ K_{\alpha\beta} & K_{\beta\beta} & K_{\beta\gamma} \\ K_{\alpha\gamma} & K_{\beta\gamma} & K_{\gamma\gamma} \end{bmatrix}\begin{bmatrix} \alpha \\ \beta \\ \gamma \end{bmatrix} + g \cdot m \cdot r_{h,stationary} \cdot \hat{k} \quad [2\text{-}33]$$

where K_{ij} represents the passive stiffness in i due to movement in j (for $i, j = \alpha, \beta, or\ \gamma$), stiffness was assumed to be symmetric ($K_{ij} = K_{ji}$), and g represents the gravitational acceleration. Vector $r_{h,stationary}$ represents r_h in the stationary frame:

$$r_{h,stationary} = \left[[R_\gamma][R_\beta][R_\alpha]\right]^T \begin{bmatrix} 0 \\ -l \\ 0 \end{bmatrix} \quad [2\text{-}34]$$

The potential energy can be re-written as:

$$\begin{aligned} V = {} & \alpha\left(\alpha K_{\alpha\alpha} + \beta K_{\alpha\beta} + \gamma K_{\alpha\gamma}\right) + \beta\left(\alpha K_{\alpha\beta} + \beta K_{\beta\beta} + \gamma K_{\beta\gamma}\right) + \gamma\left(\alpha K_{\alpha\gamma} + \beta K_{\beta\gamma} + \gamma K_{\gamma\gamma}\right) \\ & - gml(\cos\alpha \sin\gamma + \sin\alpha \sin\beta \cos\gamma) \end{aligned} \quad [2\text{-}35]$$

The Lagrangian, defined as $L = T - V$, was differentiated with respect to the time derivative of generalized coordinate:

$$\begin{aligned} \frac{\partial L}{\partial \dot{\alpha}} = {} & \frac{ml^2}{2}\left\{2\sin\beta\,(\dot{\gamma} + \dot{\alpha}\sin\beta) - 2\cos\beta\sin\gamma\left(\dot{\beta}\cos\gamma - \dot{\alpha}\cos\beta\sin\gamma\right)\right\} + I_{Ay}\dot{\alpha} \\ & + I_{hx}\sin\beta\,(\dot{\gamma} + \dot{\alpha}\sin\beta) + I_{hy}\cos\beta\cos\gamma\left(\dot{\beta}\sin\gamma + \dot{\alpha}\cos\beta\cos\gamma\right) \\ & - I_{hz}\cos\beta\sin\gamma\left(\dot{\beta}\cos\gamma - \dot{\alpha}\cos\beta\sin\gamma\right) \end{aligned} \quad [2\text{-}36]$$

$$\begin{aligned} \frac{\partial L}{\partial \dot{\beta}} = {} & ml^2\cos\gamma\left(\dot{\beta}\cos\gamma - \dot{\alpha}\cos\beta\sin\gamma\right) + I_{hy}\sin\gamma\left(\dot{\beta}\sin\gamma + \dot{\alpha}\cos\beta\cos\gamma\right) \\ & + I_{hz}\cos\gamma\left(\dot{\beta}\cos\gamma - \dot{\alpha}\cos\beta\sin\gamma\right) \end{aligned} \quad [2\text{-}37]$$

$$\frac{\partial L}{\partial \dot{\gamma}} = ml^2(\dot{\gamma} + \dot{\alpha}\sin\beta) + I_{hx}(\dot{\gamma} + \dot{\alpha}\sin\beta) \quad [2\text{-}38]$$

Taking the time derivatives of these derivatives and simplifying yields

$$\frac{d}{dt}\left(\frac{\partial L}{\partial \dot{\alpha}}\right) = I_{Ay}\ddot{\alpha} + (I_{hx} + ml^2)\left[\dot{\beta}\cos\beta\,(\dot{\gamma} + \dot{\alpha}\sin\beta) + \sin\beta\,(\ddot{\gamma} + \ddot{\alpha}\sin\beta + \dot{\alpha}\dot{\beta}\cos\beta)\right]$$
$$+ I_{hy}\left[-\dot{\beta}\sin\beta\cos\gamma\,(\dot{\beta}\sin\gamma + \dot{\alpha}\cos\beta\cos\gamma)\right.$$
$$- \dot{\gamma}\cos\beta\sin\gamma\,(\dot{\beta}\sin\gamma + \dot{\alpha}\cos\beta\cos\gamma)$$
$$+ \cos\beta\cos\gamma\,(\ddot{\alpha}\cos\beta\cos\gamma + \ddot{\beta}\sin\gamma + \dot{\beta}\dot{\gamma}\cos\gamma - \dot{\alpha}\dot{\beta}\sin\beta\cos\gamma$$
$$\left.- \dot{\alpha}\dot{\gamma}\cos\beta\sin\gamma)\right] \qquad [2\text{-}39]$$
$$+ (I_{hz} + ml^2)\left[\dot{\beta}\sin\beta\sin\gamma\,(\dot{\beta}\cos\gamma - \dot{\alpha}\cos\beta\sin\gamma)\right.$$
$$- \dot{\gamma}\cos\beta\cos\gamma\,(\dot{\beta}\cos\gamma - \dot{\alpha}\cos\beta\sin\gamma)$$
$$- \cos\beta\sin\gamma\,(-\ddot{\alpha}\cos\beta\sin\gamma + \ddot{\beta}\cos\gamma - \dot{\beta}\dot{\gamma}\cos\gamma + \dot{\alpha}\dot{\beta}\sin\beta\sin\gamma$$
$$\left.- \dot{\alpha}\dot{\gamma}\cos\beta\cos\gamma)\right]$$

$$\frac{d}{dt}\left(\frac{\partial L}{\partial \dot{\beta}}\right) = (I_{hz} + ml^2)\left[\cos\gamma(\ddot{\beta}\cos\gamma - \dot{\beta}\dot{\gamma}\sin\gamma - \ddot{\alpha}\cos\beta\sin\gamma + \dot{\alpha}\dot{\beta}\sin\beta\sin\gamma\right.$$
$$\left.- \dot{\alpha}\dot{\gamma}\cos\beta\cos\gamma) - \dot{\gamma}\sin\gamma\,(\dot{\beta}\cos\gamma - \dot{\alpha}\cos\beta\sin\gamma)\right]$$
$$+ I_{hy}\dot{\gamma}\cos\gamma\,(\dot{\beta}\sin\gamma + \dot{\alpha}\cos\beta\cos\gamma) \qquad [2\text{-}40]$$
$$+ I_{hy}\sin\gamma\,(\ddot{\beta}\sin\gamma + \dot{\beta}\dot{\gamma}\cos\gamma + \ddot{\alpha}\cos\beta\cos\gamma - \dot{\alpha}\dot{\beta}\sin\beta\cos\gamma$$
$$- \dot{\alpha}\dot{\gamma}\cos\beta\sin\gamma)$$

$$\frac{d}{dt}\left(\frac{\partial L}{\partial \dot{\gamma}}\right) = (I_{hx} + ml^2)(\ddot{\gamma} + \ddot{\alpha}\sin\beta + \dot{\alpha}\dot{\beta}\cos\beta) \qquad [2\text{-}41]$$

Solving for $\frac{\partial L}{\partial \alpha}$, $\frac{\partial L}{\partial \beta}$, and $\frac{\partial L}{\partial \gamma}$ yields

$$\frac{\partial L}{\partial \alpha} = -K_{\alpha\alpha}\alpha - K_{\alpha\beta}\beta - K_{\alpha\gamma}\gamma - mgl(\sin\gamma\sin\alpha - \cos\gamma\cos\alpha\sin\beta) \qquad [2\text{-}42]$$

$$\frac{\partial L}{\partial \beta} = \dot{\alpha}\cos\alpha\,(I_{hx} + ml^2)(\dot{\gamma} + \dot{\alpha}\sin\beta) - I_{hy}\dot{\alpha}\cos\gamma\sin\beta\,(\dot{\beta}\sin\gamma + \dot{\alpha}\cos\beta\cos\gamma)$$
$$+ \dot{\alpha}\sin\beta\sin\gamma\,(I_{hz} + ml^2)(\dot{\beta}\cos\gamma - \dot{\alpha}\cos\beta\sin\gamma) + mgl\cos\beta\cos\gamma\sin\alpha \qquad [2\text{-}43]$$
$$- K_{\alpha\beta}\alpha - K_{\beta\beta}\beta - K_{\beta\gamma}\gamma$$

$$\frac{\partial L}{\partial \gamma} = \left(I_{hy} - I_{hz} - ml^2\right)\left(\dot{\beta}\sin\gamma + \dot{\alpha}\cos\beta\cos\gamma\right)\left(\dot{\beta}\cos\gamma - \dot{\alpha}\cos\beta\sin\gamma\right) + mgl(\cos\gamma\cos\alpha - \sin\beta\sin\gamma\sin\alpha) - K_{\alpha\gamma}\alpha - K_{\beta\gamma}\beta - K_{\gamma\gamma}\gamma \quad [2\text{-}44]$$

Incorporating these expressions into Lagrange's equation (Equation 2-17) produces the equations of motion for this system. These equations were simplified by centering the moments of inertia of the hand about the wrist joint center instead of the COM of the hand. The new inertia matrix is denoted as I_H and was computed using the following relation:

$$[I_H] = [I_h] + m\{d^T d[I] - dd^T\} \quad [2\text{-}45]$$

where $[I]$ is the identity matrix and d is the vector from the wrist joint center to the COM of the hand (i.e. in this case $d = r_h$). This results in the following relationships, which are incorporated into the above equations:

$$I_{Hx} = I_{hx} + ml^2 \quad [2\text{-}46]$$

$$I_{Hy} = I_{hy} \quad [2\text{-}47]$$

$$I_{Hz} = I_{hz} + ml^2 \quad [2\text{-}48]$$

Writing the equations of motion in matrix format yields:

$$\begin{bmatrix} M_\alpha \\ M_\beta \\ M_\gamma \end{bmatrix} = \begin{bmatrix} A & B & C \\ B & D & E \\ C & E & F \end{bmatrix} \begin{bmatrix} \ddot{\alpha} \\ \ddot{\beta} \\ \ddot{\gamma} \end{bmatrix} + \begin{bmatrix} G \\ H \\ I \end{bmatrix} + \begin{bmatrix} B_{\alpha\alpha} & B_{\alpha\beta} & B_{\alpha\gamma} \\ B_{\beta\alpha} & B_{\beta\beta} & B_{\beta\gamma} \\ B_{\gamma\alpha} & B_{\gamma\beta} & B_{\gamma\gamma} \end{bmatrix} \begin{bmatrix} \dot{\alpha} \\ \dot{\beta} \\ \dot{\gamma} \end{bmatrix} + \begin{bmatrix} K_{\alpha\alpha} & K_{\alpha\beta} & K_{\alpha\gamma} \\ K_{\alpha\beta} & K_{\beta\beta} & K_{\beta\gamma} \\ K_{\alpha\gamma} & K_{\beta\gamma} & K_{\gamma\gamma} \end{bmatrix} \begin{bmatrix} \alpha \\ \beta \\ \gamma \end{bmatrix}$$

$$+ glm \begin{bmatrix} \sin\alpha \sin\gamma - \cos\alpha \cos\gamma \sin\beta \\ -\cos\beta \cos\gamma \sin\alpha \\ \sin\alpha \sin\beta \sin\gamma - \cos\alpha \cos\gamma \end{bmatrix} \qquad [2\text{-}49]$$

where variables A-G are given in Table 2-1 and parameter values are given in Table 2-2.

Table 2-2: 3-DOF model parameters

A	$I_{Hx}\sin^2\beta + I_{Hy}\cos^2\beta\cos^2\gamma + I_{Hz}\sin^2\gamma\cos^2\beta + I_{Ay}$
B	$\cos\gamma\cos\beta\sin\gamma\left(I_{Hy} - I_{Hz}\right)$
C	$I_{Hx}\sin\beta$
D	$I_{Hy}\sin^2\gamma + I_{Hz}\cos^2\gamma$
E	0
F	I_{Hx}
G	$I_{Hx}\left[\dot{\beta}\cos\beta\left(\dot{\gamma} + 2\dot{\alpha}\sin\beta\right)\right] + I_{Hy}\left[\cos\beta\cos\gamma\left(\dot{\beta}\dot{\gamma}\cos\gamma - \dot{\alpha}\dot{\beta}\sin\beta\cos\gamma - \dot{\alpha}\dot{\gamma}\cos\beta\sin\gamma\right)\right.$ $\left. - \left(\dot{\beta}\sin\gamma + \dot{\alpha}\cos\beta\cos\gamma\right)\left(\dot{\beta}\sin\beta\cos\gamma + \dot{\gamma}\cos\beta\sin\gamma\right)\right]$ $+ I_{Hz}\left[\cos\beta\sin\gamma\left(\dot{\beta}\dot{\gamma}\sin\gamma + \dot{\alpha}\dot{\gamma}\cos\beta\cos\gamma - \dot{\alpha}\dot{\beta}\sin\beta\sin\gamma\right)\right.$ $\left. + \left(\dot{\beta}\cos\gamma - \dot{\alpha}\cos\beta\sin\gamma\right)\left(\dot{\beta}\sin\beta\sin\gamma - \dot{\gamma}\cos\beta\cos\gamma\right)\right]$
H	$-I_{Hx}\dot{\alpha}\cos\beta\left(\dot{\gamma} + \dot{\alpha}\sin\beta\right)$ $+ I_{Hy}\left[\dot{\alpha}\sin\beta\cos\gamma\left(\dot{\beta}\sin\gamma + \dot{\alpha}\cos\beta\cos\gamma\right)\right.$ $\left. + \dot{\gamma}\cos\gamma\left(2\dot{\beta}\sin\gamma + \dot{\alpha}\cos\beta\cos\gamma\right) - \dot{\alpha}\sin\gamma\left(\dot{\beta}\sin\beta\cos\gamma + \dot{\gamma}\cos\beta\sin\gamma\right)\right]$ $+ I_{Hz}\left[\dot{\alpha}\sin\beta\sin\gamma\left(\dot{\alpha}\cos\beta\sin\gamma - \dot{\beta}\cos\gamma\right)\right.$ $\left. + \dot{\alpha}\cos\gamma\left(\dot{\beta}\sin\beta\sin\gamma - \dot{\gamma}\cos\beta\cos\gamma\right) - \dot{\gamma}\sin\gamma\left(2\dot{\beta}\cos\gamma - \dot{\alpha}\cos\beta\sin\gamma\right)\right]$
I	$I_{Hx}\left(\dot{\alpha}\dot{\beta}\cos\beta\right) + \left(I_{Hy} - I_{Hz}\right)\left(\dot{\beta}\sin\gamma + \dot{\alpha}\cos\beta\cos\gamma\right)\left(\dot{\alpha}\cos\beta\sin\gamma - \dot{\beta}\cos\gamma\right)$

Table 2-3: Mean male and female model parameters

Parameter	Male	Female
m [kg]	0.439	0.346
l [m]	0.0665	0.0586
I_{Hx} [kgm^2]	0.00317	0.00180
I_{Hy} [kgm^2]	0.000501	0.000241
I_{Hz} [kgm^2]	0.00276	0.00164
I_{Ay} [kgm^2]	0.00137	0.000505
$K_{\alpha\alpha}$ [Nm/rad]	0.756	0.827
$K_{\alpha\beta} = K_{\beta\alpha}$ [Nm/rad]	0.0175	0.0809
$K_{\alpha\gamma} = K_{\gamma\alpha}$ [Nm/rad]	0.291	0.148
$K_{\beta\beta}$ [Nm/rad]	0.992	0.713
$K_{\beta\gamma} = K_{\gamma\beta}$ [Nm/rad]	-0.0991	-0.0780
$K_{\gamma\gamma}$ [Nm/rad]	2.92	2.24
$B_{\alpha\alpha}$ [Nms/rad]	0.0236	0.0362
$B_{\alpha\beta} = B_{\beta\alpha}$ [Nms/rad]	0.000791	0.00376
$B_{\alpha\gamma} = B_{\gamma\alpha}$ [Nms/rad]	0.00831	0.00643
$B_{\beta\beta}$ [Nms/rad]	0.0300	0.0300
$B_{\beta\gamma} = B_{\gamma\beta}$ [Nms/rad]	-0.00316	-0.00351
$B_{\gamma\gamma}$ [Nms/rad]	0.0882	0.0959

3 CONTROL OF REDUNDANT WRIST AND FOREARM MOVEMENTS

A great deal of prior research has attempted to explain how the neuromuscular system controls body members. This has been investigated primarily in for reaching movements involving the shoulder and arm, and has resulted in several hypotheses with various levels of success. Our research presented in Chapter 2 suggests that wrist and forearm dynamics are significantly different from the shoulder and arm, with stiffness dominating instead of inertia. Under this premise it is necessary to reexamine the neuromuscular control strategies used in this vastly different system. Note: the experimental portion of this chapter was conceived, planned and conducted by Garrett Dorman (Section 3.2.1 Subjects throughProtocol)

3.1 Introduction

When making upper limb movements, humans often recruit more degrees of freedom (DOF) than are necessary, allowing the same posture to be achieved in an infinite variety of configurations. How the neuromuscular system deals with such kinematic redundancy has been studied extensively for reaching movements; common trajectories (selected from the infinite variety of possibilities) have been shown to be similar to trajectories that minimize a cost function associated with movement (such endpoint error or torque change) or maximize an attribute of movement (such as stability).

In contrast, how the neuromuscular system solves the problem of redundancy for wrist and forearm movements is unknown. The wrist and forearm allow significant movement in three

DOF: flexion-extension (FE), radial-ulnar deviation (RUD), and pronation-supination (PS). Many tasks involving FE, RUD, and PS, such as pointing, require less than three DOF. While pointing could be achieved with FE and RUD alone, subjects repeatedly recruit pronation-supination (PS) in addition to FE and RUD. Why does the neuromuscular system recruit PS even though it is not necessary?

The purpose of this study is to 1) characterize the use of PS during pointing movements and 2) determine why PS is used (even though it is not necessary). More specifically, we tested whether the pattern of PS matched that predicted by a motor control strategy that minimized a cost function (path length, potential energy, work, or effort), or whether the pattern simply resulted from mechanical interaction between DOF.

We found that subjects did indeed use a statistically non-zero amount of PS during pointing movements. The amount of PS was repeatable within and between subjects and varied sinusoidally with target direction. Furthermore, this pattern depended on movement amplitude but not movement speed. When compared to the patterns of PS recruitment predicted for minimizing common cost functions and for mechanical interaction, the observed pattern of PS recruitment matched the pattern predicted for mechanical interaction, but not the patterns predicted for minimizing common cost functions.

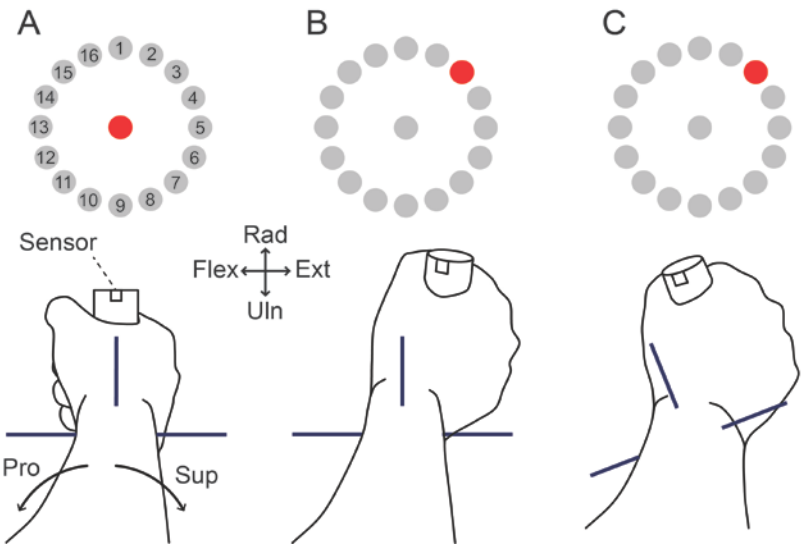

Figure 3-1: Subjects made 800 center-out movements to 16 targets in the periphery, incorporating both comfortable and fast speeds as well as to smaller and larger radii (15°and 22.5°).

3.2 Methods

3.2.1 Experiment

Subjects

Ten young, healthy, right-handed subjects (5 female, 21-28 years old) participated in this experiment. None of the subjects suffered from neurological injury or biomechanical injury to the wrist or forearm. Following procedures approved by Brigham Young University's Institutional Review Board, informed consent was obtained from all subjects.

Experimental Setup

Subjects were seated in a chair with the right arm in the parasagittal plane. The shoulder was in approximately 20° of flexion and 0° abduction and humeral rotation, and the elbow in approximately 30° of flexion. A shoulder belt constrained shoulder motion. The proximal 10cm of the forearm rested on a horizontal support, constraining elbow motion but allowing unobstructed forearm rotation. In their right hand, subjects held a lightweight handle to which a

motion sensor (trakSTAR by Ascension Technologies, Burlington, VT) was rigidly attached. A second motion sensor was fastened to the dorsal aspect of the distal forearm, approximately 4cm proximal to the center of the wrist joint. Together these motion sensors measured wrist flexion-extension (FE) and radial-ulnar deviation (RUD) as well as forearm pronation-supination (PS) at approximately 300Hz with an angular accuracy and resolution of 0.5° and 0.1°, respectively. At a combined weight of approximately 75g (roughly 5% of the mass of an average hand and forearm), the handle and two sensors presented negligible interference to natural wrist and forearm movements.

In front of the subject was a monitor with 16 peripheral targets equally distributed around a center target. Also displayed was a cursor that represented the direction in which the hand pointed, similar to the projection of a laser pointer on a screen. More specifically, the horizontal and vertical screen coordinates of the cursor were calculated as

$$x_s = C[-cos(\alpha)sin(\beta)cos(\gamma) + sin(\alpha)sin(\gamma)] \quad [3\text{-}1]$$

$$y_s = C[-sin(\alpha)sin(\beta)cos(\gamma) - cos(\alpha)sin(\gamma)] \quad [3\text{-}2]$$

where C is a constant factor to adjust the cursor coordinates to the size of the monitor, and α, β, and γ are Euler angles representing pronation, flexion, and ulnar deviation (in that order), with negative values indicating supination, extension, and radial deviation (see Section 3.5 for derivation). As for pointing with a laser pointer, the position of the cursor depended on PS (as well as FE and RUD), allowing the cursor to reach the same target with different combinations of FE, RUD, and PS. To go from the center target to any of the peripheral targets required either 15° or 22.5° of displacement in the pointing direction of the hand (depending on the session). The cursor was calibrated to be in the center target when the wrist and forearm were in neutral position, defined as follows. The forearm was in neutral PS when the dorsal aspect of the distal

forearm (more specifically the dorsal tubercle of the radius and the dorsal-most protuberance of the ulnar head) was in the parasagittal plane. The wrist was in neutral FE when the handle, the center of the wrist joint, and the midpoint between the medial and lateral epicondyles were aligned. Finally, the wrist was in neutral RUD when the center of the head of the third metacarpal, the center of the wrist joint, and the lateral epicondyle were aligned. This definition of neutral position is similar to the ISB recommendation for global movements (Wu et al., 2005) except that the definition of FE was adjusted to account for the fact that subjects were holding a handle.

Protocol

Subjects participated in four experiments divided into two sessions in which they were required subjects to combine FE, RUD, and PS in order to move the cursor between the center target and each peripheral target. No instruction was given regarding how to combine these three DOF. The two experiments in each session were identical except that subjects were instructed to move either at a comfortable speed or as fast as possible. The order of the experiments within each session was randomized, and there was a break of 5 minutes between experiments. Moving between the center target and any of the peripheral targets required 15° of rotation in the first session, and each subject was required to complete this 15 times, for a total of 240 roundtrip movements. In the second session targets required 22.5° of rotation and were required 10 times, for a total of 160 movements. Each session lasted approximately 40 min.

Data processing

Only outbound movements were included in the analysis. Because PS was not prescribed or graphically displayed (besides its effect on the pointing direction of the hand), subjects exhibited significant drift in PS over the duration of a session. To remove the effect of this drift

on the observed pattern of PS recruitment, we calculated for each movement the variable Δp as the final PS angle minus the initial PS angle (Figure 3-2). The large majority of movements were roughly monotonic for PS, with only slight overshoot at the end of a movement at the end of each movement. We also calculated the target angle θ, adjusted to account for the drift in PS as shown in Figure 3-2.

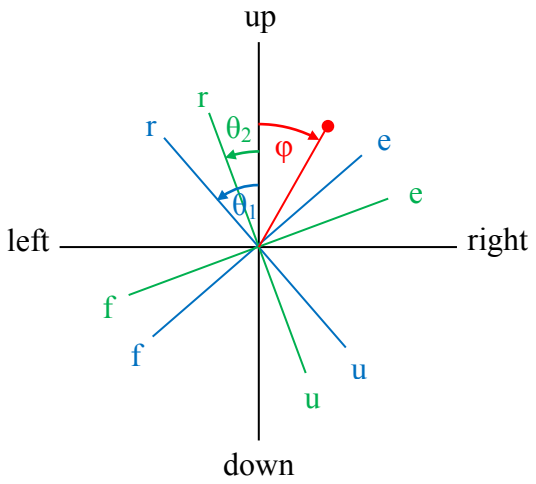

Figure 3-2: Calculation of the change in PS, ΔPS, and the target angle, θ. The black coordinate frame represents the extrinsic (world-space) frame, while the blue and green frames represent the intrinsic (joint-space) frame at the beginning and end of a move, respectively. Since the start and end orientations are θ_1 and θ_2, respectively, the value of ΔPS is $\theta_2 - \theta_1$. If the target is shown as the red dot, then the target angle associated with this movement is $\theta = \theta_1 + \phi$.

Data analysis

To identify possible trends in the resultant data, the ΔPS values were compared against the angle of the target location. The ΔPS values from all four experimental sessions for each subject were first pooled, and outliers removed that were more than 2σ from the mean value. The mean bias was then removed from the remaining data points. The resultant data exhibited a

generally sinusoidal trend, to which a least squared sinusoidal fit was superimposed in the form of $\Delta PS = A\sin(B\theta + C)$ where A is the amplitude, B is the frequency, and C is the phase shift.

3.2.2 Simulation

To provide insight into possible control strategies employed by the neuromuscular system for the wrist and forearm, the aforementioned experiment was simulated using a 3 DOF model of wrist and forearm dynamics (Hill, 1968). In this simulation, all anthropometric model parameters, including stiffness, inertial, and damping values, were taken from a similar experiment involving 5 male and 5 female subjects (Peaden and Charles). Male and female values were averaged to obtain non gender-specific results. Theoretical target positions for this experiment would lie on a continuous circle with a radius defined by a 15° wrist rotation in either FE or RUD and centered on the neutral position. Due to the relative simplicity of simulation, this allows for a higher resolution than the 16 points chosen for experimentation, and 72 evenly spaced "virtual targets" were placed on this circle at 5° increments, starting from pure radial deviation and proceeding around the circle in a clockwise fashion. The amount of PS recruited at each virtual target in each simulation was recorded.

As in the experiment, the wrist was under-constrained in the simulation. The wrist model possesses three unknown variables, one per DOF, but only two constraints, one for each coordinate of the pointing direction, leaving one variable undefined. Since the pointing direction of the wrist cannot be uniquely solved for in this scenario (infinite solutions are possible), various hypotheses were tested to provide the needed relationships between the several DOF, such that each hypothesis had a unique solution at each target. These hypotheses fall into two principal categories: cost function hypotheses, which assume that the neuromuscular system is

attempting to minimize some perceived movement cost, and Two DOF hypotheses, which assume that the neuromuscular system primarily concerns itself with FE and RUD.

Cost Function Hypotheses

A great variety of movement costs could be examined which would drive the neuromuscular system to select a unique joint path with the three DOF of the wrist and forearm. Five such costs were selected based on their intuitive connection to physiological behavior. The selected costs include mechanical work, movement effort, end-point effort, change in potential energy, and path length. The first two of these hypotheses are path dependent and require full motion simulation, whereas the second three only require a steady state solution.

Mechanical Work

The idea that the neuromuscular system attempts to conserve energy in movement is long standing and has been shown to be accurate in some scenarios (Alexander, 1997). The cost associated with energy conservation used here is mechanical work, which is the amount of mechanical energy the body produces to execute the movement. Energy expenses resulting from non-mechanical aspects of the system (e.g. chemical processes) are not considered under this assumption. This hypothesis is therefore akin to the neuromuscular system choosing the path of least physical resistance.

To test this hypothesis a function was programmed into OptdesX, a commercial software optimizer. The function used the 3DOF model to simulate a movement which started at the neutral position ($\alpha = \beta = \gamma = 0$) and followed a minimum-jerk velocity profile for each joint angle until terminating at a set of joint angles chosen by the optimizer. The movement duration was set to 0.5 seconds, and the applied forces necessary to execute the movement were calculated in 0.001 second step intervals. Each optimization was also constrained, so that the

wrist pointed no more than 0.057° off from each "virtual target" at the endpoint, and so that joint angles could not exceed reasonable values (FE and RUD constrained to ±30°, PS constrained to ±80°). The optimizer would iterate on this function until it found a set of joint angles which minimized the mechanical work without violating these constraints. Sequential quadratic programing (SQP) and generalized reduced gradient (GRG) algorithms were both used on each data point to provide confidence in the result. The solution found at various virtual targets was also further verified by repeating the optimization from different initial conditions to verify that an absolute minimum had been found within the constraints. Mechanical work was calculated as a numerical approximation of:

$$C_{work} = \int_0^{\alpha_f} M_\alpha \delta\alpha + \int_0^{\beta_f} M_\beta \delta\beta + \int_0^{\gamma_f} M_\gamma \delta\gamma \qquad [3\text{-}3]$$

Where α_f, β_f, and γ_f are the joint angles at the virtual target.

Movement Effort

The neuromuscular system may also attempt to find a path in which it has to exert the least amount of effort, defined here as joint torque. This differs from minimizing work in that the displacements produced by the applied torques have no direct effect on the cost, making longer joint paths potentially more favorable if they provide less net resistance. Effort cost is defined as the net effort required for the movement, which is the integral of the magnitude of the torque vector taken across the entire movement, from the start time, $t = 0$, until movement completion at $t = t_f$:

$$C_{effort} = \int_0^{t_f} \sqrt{M_\alpha^2 + M_\beta^2 + M_\gamma^2 + 2M_\alpha M_\gamma \sin(\beta)}\, dt \qquad [3\text{-}4]$$

To minimize the movement effort the same methods were employed as in minimizing work, only that the OptdesX function was modified to compute effort as defined above.

Postural Effort

Instead of following a path that minimizes net effort, this hypothesis assumes that the neuromuscular system attempts to minimize the effort required to maintain the end effector pointed to the correct target. This effort can be computed from the magnitude of the torque vector used to sustain this position:

$$C_{postural-effort} = \sqrt{M_{\alpha_f}^2 + M_{\beta_f}^2 + M_{\gamma_f}^2 + 2M_{\alpha_f}M_{\gamma_f}\sin(\beta_f)} \quad [3\text{-}5]$$

To determine the required torques in this equation only the static terms from the 3 DOF wrist model need to be considered:

$$\begin{bmatrix} M_\alpha \\ M_\beta \\ M_\gamma \end{bmatrix} = \begin{bmatrix} K_{\alpha\alpha} & K_{\alpha\beta} & K_{\alpha\gamma} \\ K_{\alpha\beta} & K_{\beta\beta} & K_{\beta\gamma} \\ K_{\alpha\gamma} & K_{\beta\gamma} & K_{\gamma\gamma} \end{bmatrix} \begin{bmatrix} \alpha \\ \beta \\ \gamma \end{bmatrix} + g l_1 m_h \begin{bmatrix} \sin\alpha \sin\gamma - \cos\alpha \cos\gamma \sin\beta \\ -\cos\beta \cos\gamma \sin\alpha \\ \sin\alpha \sin\beta \sin\gamma - \cos\alpha \cos\gamma \end{bmatrix} \quad [3\text{-}6]$$

The required effort can therefore be determined from the above equation if all joint angles are considered in their final state, α_f, β_f, and γ_f. The required joint angles are also constrained in that they must point to the correct virtual target. These relationships can be obtained by solving for x and y in Equations 3-1 and 3-2, resulting in the following relationships with the joint angles:

$$\gamma = -\sin^{-1}(\cos(\alpha) * y_s - \sin(\alpha) * x_s) \quad [3\text{-}7]$$

$$\beta = \sin^{-1}\left(\frac{\sin(\alpha) * \sin(\gamma) - x_s}{\cos(\alpha) * \cos(\gamma)}\right) \quad [3\text{-}8]$$

These two equations, combined with a minimization of the effort cost function, provide an equal number of relations and unknowns, indicating that a solution can be found. To compute this optimum all possible values of α were considered from $-\pi/2$ to $\pi/2$, and γ and β were made dependent on this value. The cost function was then computed along this continuum at each virtual target, the minimum found, and the corresponding joint angles recorded.

Change in Potential Energy

The body may concern itself most with the work required to maintain its endpoint position rather than just attain it. Since dissipated energy (damping) will not affect this, then it may be computed as a change in the potential energy between this state and the neutral position. This relationship is found in the derivation of the 3 DOF wrist and forearm model (Peaden and Charles, Appendix p3).

This cost function was optimized using the same methods described for the end-point effort hypothesis, with change in potential energy as the computed cost. Specifically, the change in potential energy was computed with the aid of Equations 3-7 and 3-8 for all possible values of α from $-\pi/2$ to $\pi/2$ until the minimum was found.

Path Length

Under the assumption that path length is the highest cost which the neuromuscular system must account for, a joint path will be chosen which minimizes the rotation of the coordinate frame from its neutral position. Combining the rotation matrix which moves the hand to point each virtual target from neutral position (see Section 3.5) with the equation for equivalent angle-axis representation of joint rotations (Eqn. 2.81, Craig, 2004, p 47) this angular rotation can be shown to be:

$$C_{length} = \left|\cos^{-1}\left(\frac{(\cos\alpha * \cos b)}{2} + \frac{(\cos\alpha * \cos g)}{2} + \frac{(\cos b * \cos g)}{2} - \frac{\sin\alpha \sin\beta \sin\gamma}{2} - \frac{1}{2}\right)\right| \quad [3\text{-}9]$$

This change in potential energy was minimized as a cost function using the same methods employed to minimize end-point effort and change in potential energy.

Mechanical Interaction Hypothesis

Although PS, FE, and RUD all affect the pointing direction, they do not contribute equally to the task of reaching the target. While some targets can be reached by FE alone and others by RUD alone, and all targets can be reached by a combination of FE and RUD, no target can reached by PS alone, nor is PS actually necessary to reach any target. Indeed, linearizing Eq. 3-1 and 3-2 yields $x \approx -f$ and $y \approx -u$. Therefore, one potential strategy of the neuromuscular system may be to simply ignore PS (intentionally or not) and try to reach targets with FE and RUD alone. However, because PS is mechanically coupled with FE and RUD, torques in FE and RUD will create movement in PS. We hypothesize that the observed behavior in PS may simply be this movement, passively and secondarily induced by a control strategy that did not involve PS.

To test this hypothesis, we ignored PS during the planning stage and computed the effect on PS during the execution stage. With only 2 available DOF, the planning stage reduces to a fully constrained problem, so we determined the FE and RUD angles and torques necessary to reach a virtual target by inverse simulation using a 2-DOF model of the wrist, and then executed the movement by forward simulation using the full 3-DOF model of the wrist and forearm (with zero input torque in PS; Figure 3-3). Without a stabilizing torque in PS, mechanical interaction between the DOF caused a "kickback displacement" in PS, which was determined at each virtual target.

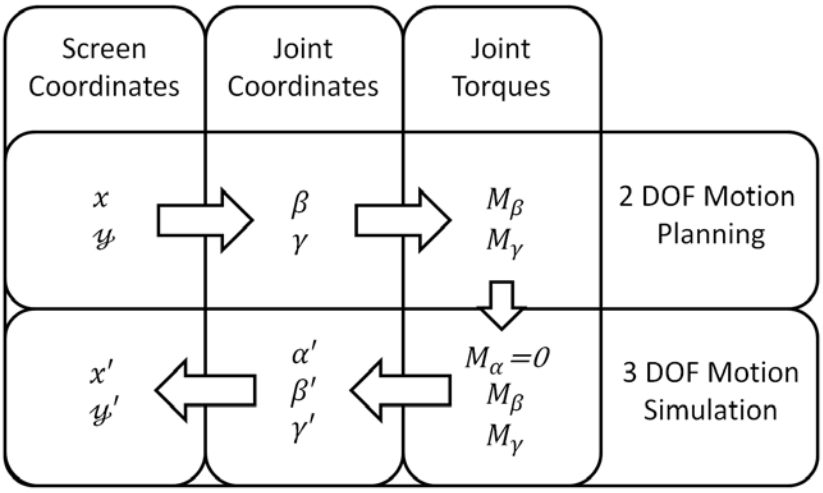

Figure 3-3: Methodology for computing the kinematics predicted by the interaction hypothesis.

Because the movement in PS was not taken into account in the planning stage, the actual final pointing direction was slightly different from the planned direction. The error in pointing direction was small (mean error = 1.2°, maximum error = 2.7°) and in practice could be ignored (the targets had a radius of 1.5°) or corrected toward the end of the movement using visual feedback. Nevertheless, we also simulated a slight variation in control strategy that results in zero endpoint error. According to this strategy, the input torque in PS is still zero, but the torques in FE and RUD are altered during the planning stage to take the mechanical interaction with PS into account (using the full 3-DOF model). The resulting movement in PS was computed by setting the steady-state PS torque in the 3-DOF model equal to zero and combining this condition with Equations 3-3 and 3-4, resulting in a fully constrained system which was solved for p at every virtual target.

3.2.3 Comparison of Experimental and Simulated Data

The accuracy of each hypothesis was evaluated by qualitatively comparing their predicted PS values with the experimentally recorded values of ΔP. Specifically, a potentially valid hypothesis should exhibit the same behavior as the experimental data in three key areas: frequency, phase, and amplitude. The frequency of the data or hypotheses is defined as the number of times PS recruitment exhibits identical behavior that is offset only in target angle within the circle of targets. Amplitude is defined as the peak value of the absolute value of the observed or theoretical PS recruitment. Phase shift is defined as the offset in phase of the hypothesis or experimental data from a pure sinusoidal behavior. Hypotheses that appear to meet these criteria are further evaluated by observing their predicted behavior with anthropometric parameters from a similar experiment (Peaden and Charles) to verify that their predicted results do not differ substantially when considered for individuals as opposed to populations.

3.3 Results

3.3.1 Experiment

Most all subjects exhibited a clearly discernible sinusoidal trend in their PS recruitment (Figure 3-4:). After each subject's measured PS recruitment was fit to a sine curve, the mean amplitude of the sinusoid among subjects was 1.7°, with a frequency of 1.12 cycles/revolution and phase shift of 115°. There is consistency between the subjects in regard to all three of these phenomena, and almost all of the determined parameters for each subject fall within two standard deviations of the mean. Two obvious exceptions to this are with subject 2 (whose frequency is 2.80 SD from the mean) and subject 7 (whose phase is 1.98 SD from the mean) (Table 3-1). Removing these outliers, the mean frequency becomes 1.01 cycles/revolution, and the mean phase shift becomes 128°.

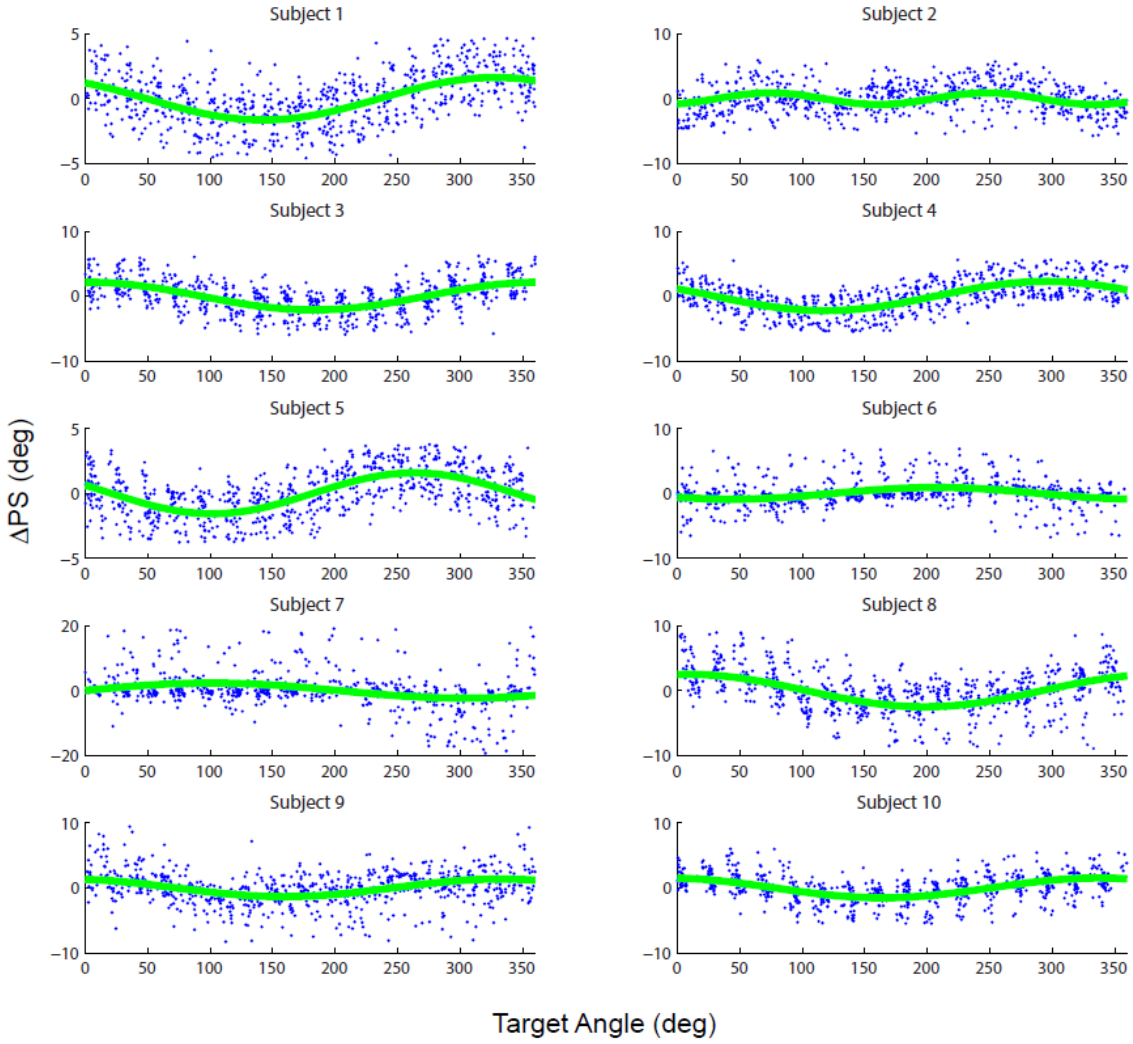

Figure 3-4: The ΔPS calculated for each subject plotted against target angle. The target corresponding to pure radial deviation was considered to be at 0°, and the angle increased in a clockwise fashion, passing through pure extension at 90°, ulnar deviation at 180°, and flexion at 270°, although target angles were possible at any point along this circle due to the compensation for PS drift. This same convention is used on all future figures.

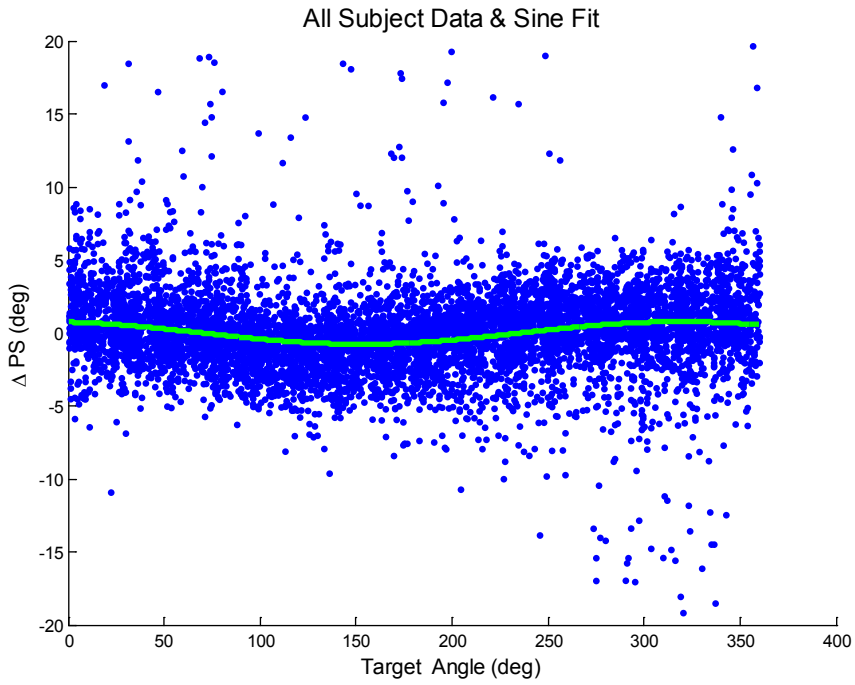

Figure 3-5: Mean ΔPS (averaged across all subjects) plotted against target angle. The sine fit to this data has an amplitude of 0.77°, a frequency of 1.08 cycles/revolution, and a phase shift of 105°.

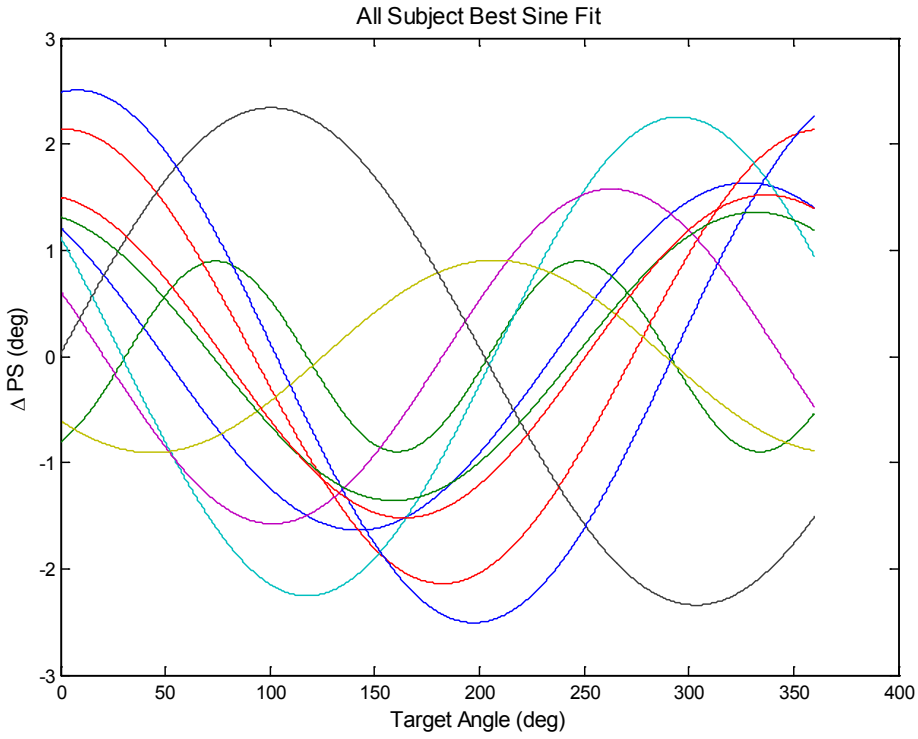

Figure 3-6: Graph of subjects' least squares sine fit approximations

Table 3-1: Least squares sine fits of subjects' ΔPS values

Subject	Amplitude ΔPS (deg)	Frequency (cycles/revolution)	Phase Shift (degrees)	Residual
1	1.64	0.970	132	1977
2	0.898	2.08	116	3560
3	2.14	0.995	88	2995
4	2.26	1.01	150	2680
5	1.58	1.11	157	1531
6	0.907	1.10	222	2780
7	2.34	0.887	1	20048
8	2.51	0.951	82	5580
9	1.36	1.04	104	4527
10	1.52	1.04	99	2509
mean	1.71	1.12	115	4819
standard deviation	0.578	0.343	58	5482

3.3.2 Simulation

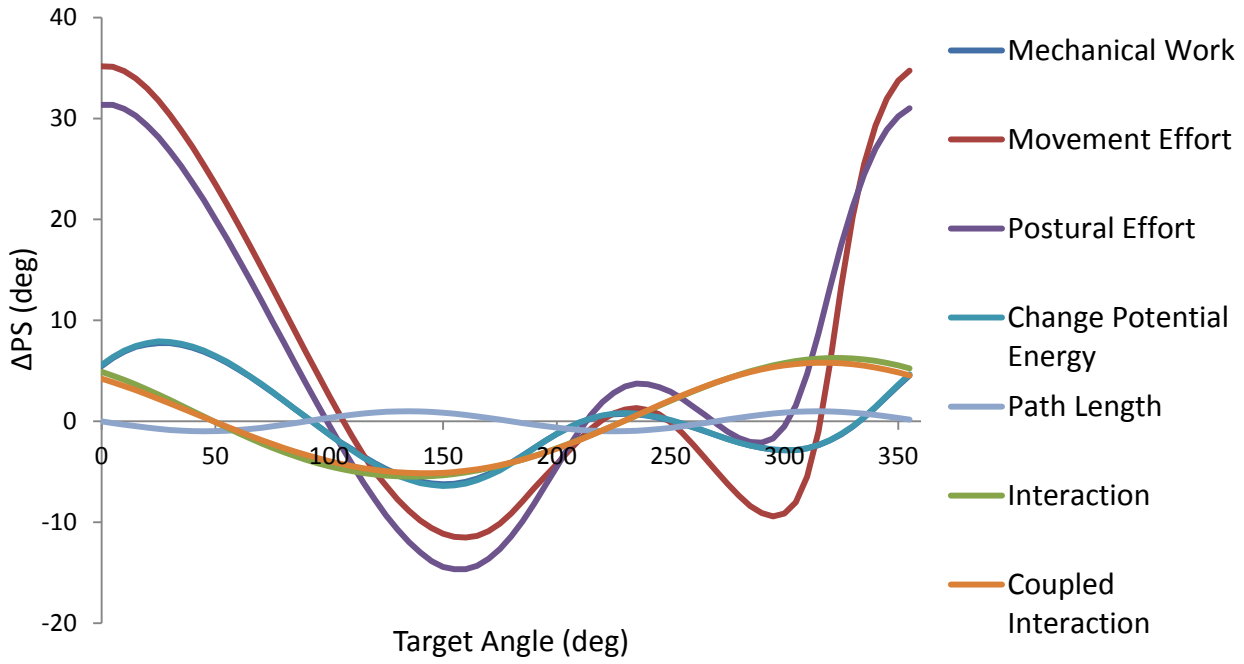

Figure 3-7: PS recruitment predicted by minimization of common cost functions and by simple mechanical interaction. Positive values in the y-axis indicate pronation, whereas negative values indicate supination. The x-axis values are the target angle for each of the 72 data points simulated for each. The target angle is defined as the angle offset from pure radial deviation (right hand), proceeding clockwise in a completed circle.

The amount of PS recruitment predicted varies greatly in behavior between the several hypotheses (Figure 3-7:). The amplitude of the various hypotheses varies between 1° when minimizing the rotation of the coordinate frame, to 35° when minimizing effort. Frequency varies between 1 cycle/rotation for most hypotheses, but 2 cycles/rotation when minimizing the rotation of the coordinate frame. Phase can only be compared when observing strictly sinusoidal curves, and varies from 131° for the interaction and coupled interaction hypothesis, to180° when minimizing the rotation of the coordinate frame. All hypotheses are cyclic; there are no discontinuities. The minimum work and minimum change in potential energy hypothesis are nearly identical, and their behavior is nearly coincident. Likewise the kickback and coupled kickback hypothesis share a nearly identical locus, but there is a slightly larger discrepancy in this case. All other hypotheses are easily distinguishable.

3.3.3 Comparison of Experimental and Simulated Data

Most hypotheses failed in one or more area, however both the interaction and coupled interaction hypothesis meet all the established requirements for a good hypothesis (Table 3-2). The interaction hypothesis is near perfect sinusoid with a frequency of 1 cycle/revolution, amplitude of 5.9°, and phase shift of 131°. The coupled interaction hypothesis produces almost identical results, only with a slightly reduced amplitude.

Despite their comparative resemblance to the experimental data, the predicted amplitude of the interaction and coupled interaction hypothesis, although of similar magnitude, remains larger than the mean value of the sinusoidal fits observed (about 1.71º ΔPS, Table 3-1). We

Table 3-2: Comparison between experimental data and various hypotheses. A good hypothesis should possess the same frequency, amplitude, and phase as the experimental data. Note that in order to have the correct phase, the theoretical curve must exhibit the same sinusoidal behavior observed experimentally, since the phase shift of dissimilar curves cannot be determined.

Hypothesis	Frequency	Amplitude	Phase
Mechanical Work	**X**	**X**	
Movement Effort	**X**		
Postural Effort	**X**		
Change in Potential Energy	**X**	**X**	
Path Length			
Interaction	**X**	**X**	**X**
Coupled Interaction	**X**	**X**	**X**

found that increasing $K_{\alpha\alpha}$ by a factor of three reduces the predicted magnitude for both hypotheses to roughly the same magnitude as the experimental data. This is plausible because it would indicate a small amount of co-contraction in the DOF least used in the movement (co-contraction may cause the stiffness to increase much more than this).

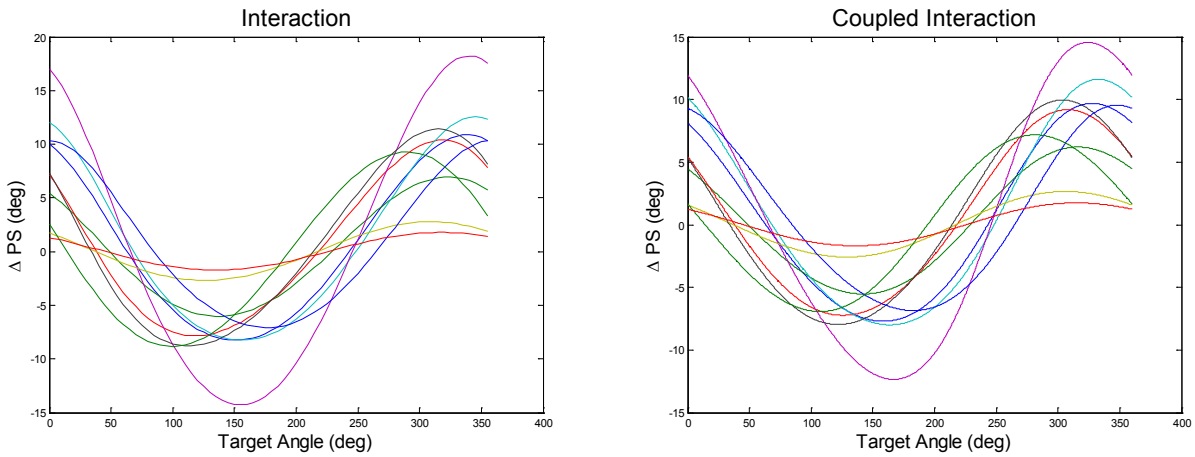

Figure 3-8: The ΔPS predicted by the interaction and coupled interaction hypotheses, based on individual anthropometric parameters from subjects in a similar experiment (Peaden and Charles). The interaction hypothesis had amplitudes ranging from 1.7° to 18° while the coupled interaction hypothesis had amplitudes ranging 1.7° to 15°. Both hypothesis phase shifts ranged from 95° to 166°.

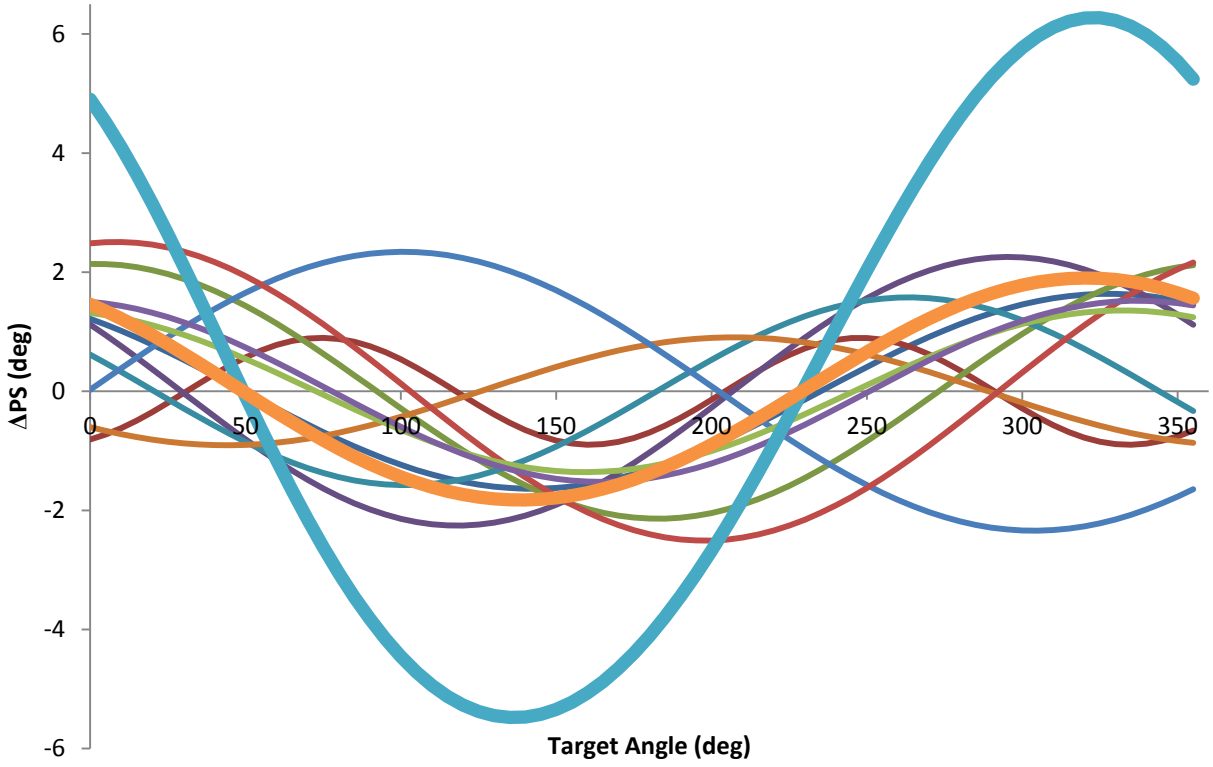

Figure 3-9: Comparison of subject least squares regression sine fits (fine lines) to the interaction hypothesis (light blue, bold line) and the interaction hypothesis with simulated co-contraction of the forearm (orange, bold line).

3.4 Discussion

Of the hypotheses tested, the interaction and coupled interaction hypotheses appear to hold the most merit. Although both hypotheses predict larger amounts of ΔPS then the experimental data suggests, when individual subjects anthropometric parameters are simulated (Figure 3-8:), the amount of ΔPS predicted becomes comparable to the spread of data observed in individual subjects (Figure 3-4:). Also, co-contraction of the forearm, likely caused by the gripping of the sensor handle, may further explain this discrepancy.

The interaction hypothesis suggests that the neuromuscular system may simplify pointing by approximating the wrist and forearm as a 2 DOF system. This implies that the neuromuscular

system may employ a simplified internal model for scenarios involving redundancy, ignoring additional complications which contribute little to accuracy—this is similar to other research, including the unconstrained manifold (Scholz and Schoner, 1999) and leading joint hypotheses (Dounskaia, 2005). The failure of the wrist and forearm to exactly attain its target in this hypothesis is of little consequence, since when it is constrained to do so as in the coupled interaction hypothesis, nearly identical results are produced.

3.5 Screen Coordinate Derivation

As defined by Peaden and Charles, the wrist and forearm's stationary coordinate frame is positioned so that from anatomical position the x-axis points in the frontal direction (roughly normal to the palm), the y-axis points upward along the forearm towards the shoulder, and the z-axis points outward parallel to the frontal plane (roughly in the thumb's pointing direction). From this coordinate system, the rotation matrix that brings a point a distance l_1 from the wrist, extending along the third metacarpal, into the stationary frame is:

$$R = \left[[R_\gamma][R_\beta][R_\alpha]\right]^T \begin{bmatrix} 0 \\ -l_1 \\ 0 \end{bmatrix} \quad [3\text{-}10]$$

Which when expanded becomes

$$R = \begin{bmatrix} \cos\beta\cos\alpha & \sin\gamma\sin\alpha - \sin\beta\cos\gamma\cos\alpha & \sin\beta\sin\gamma\cos\alpha + \cos\gamma\sin\alpha \\ \sin\beta & \cos\beta\cos\gamma & -\cos\beta\sin\gamma \\ -\cos\beta\sin\alpha & \sin\beta\sin\alpha\cos\gamma + \sin\gamma\cos\alpha & \cos\gamma\cos\alpha - \sin\beta\sin\gamma\sin\alpha \end{bmatrix} \quad [3\text{-}11]$$

Multiplying this matrix by the arbitrary wrist end point $\begin{bmatrix} 0 \\ -1 \\ 0 \end{bmatrix}$ the x, y, and z coordinates of a point on the hand a distance 1 away can be determined. This produces:

$$r_{h,stationary} = \begin{bmatrix} -\sin(\alpha)\sin(\gamma) + \cos(\alpha)\sin(\beta)\cos(\gamma) \\ -\cos(\beta)\cos(\gamma) \\ -\cos(\alpha)\sin(\gamma) - \sin(\alpha)\sin(\beta)\cos(\gamma) \end{bmatrix} \quad [3\text{-}12]$$

In the anatomical coordinate frame used by Peaden and Charles, the targets in this experiment would lie on the XZ plane, and their coordinates could be found from the first and third elements of this matrix. The screen coordinates differ from the anatomical coordinate system used in that the sign of the x-coordinate is reversed, and the y screen coordinate is equal to the z anatomical coordinate. The screen coordinates then become:

$$x_s = C[-cos(\alpha)sin(\beta)cos(\gamma) + sin(\alpha)sin(\gamma)] \quad [3\text{-}13]$$

$$y_s = C[-sin(\alpha)sin(\beta)cos(\gamma) - cos(\alpha)sin(\gamma)] \quad [3\text{-}14]$$

Where C is constant factor to adjust the cursor coordinates to the size of the monitor.

4 CONCLUSION

Despite the abundance of Repetitive Strain Injuries (RSI) to the wrist, our current understanding of wrist movement is lacking in key areas necessary to remedy this problem. Two of these areas include an improved understanding of the torques acting on the wrist, as well as the control strategies that govern wrist movement. This knowledge is essential in designing ergonomic and therapeutic devices which prevent or even cure RSI in the wrist. Because natural movement generally combines wrist movements with forearm movements, understanding the torques and control strategies involved in wrist movements requires that we understand forearm movements as well. The research presented in this thesis addresses these gaps in our current understanding by modeling dynamic wrist and forearm impedance torques, and by examining the needed complexity and possible control strategies employed by the neuromuscular system's internal model for wrist and forearm movement.

A key contribution of this research is a complete 3-DOF model of wrist and forearm dynamics, which when coupled with correct parameters can be used to both compute joint torques and predict movements from known torques. This model provides several advantages over current computational models. Specifically, it requires joint impedance (as opposed to individual muscle parameters), which can be estimated or even measured for a given subject, it is simple to implement and requires no unique software package, and it can be easily manipulated for a specific application. This model was used in all aspects of this research.

Our first experiment (Chapter 2) found that stiffness dominated the torques acting on the forearm, as well as on the wrist and forearm together, and that interaction torques between the wrist and forearm (due to impedance coupling) were significant. Therefore, in terms of dynamics, forearm rotation is more similar to wrist rotations, which are also dominated by stiffness effects (Charles and Hogan, 2011) than shoulder and elbow rotations, which are believed to be dominated by inertial effects.

Another key finding of this experiment was in modeling the torque required for small-angle movements, some torque terms contribute little to the overall torque and can be neglected with little loss in accuracy. More specifically, linearizing the equations of motion resulted in an average error of less than 1%. This suggests that an internal model for such movements does not need to be complicated. This conclusion, however, became invalid if the interaction torques between degrees of freedom (DOF) were removed, suggesting that the neuromuscular system's internal model for these movements must account for coupling between DOF. These results likewise agree with prior research considering only 2 DOF (Charles and Hogan, 2011).

In our second experiment we compared experimental and theoretical results of PS recruitment for a 2 DOF pointing task in which all 3 DOF of the wrist and forearm were available in an effort to determine how the neuromuscular system may handle joint redundancy. Our results (Chapter 3) suggest that the neuromuscular system may control the task of pointing with the wrist and forearm, which involves redundancy, with a simplified 2-DOF model. Specifically, forearm motion was the least critical to the task, and simulated motor planning that neglected this DOF produced theoretical predictions of PS usage most similar to what was observed experimentally. This agrees with prior research which has suggested that the

neuromuscular system focuses its control efforts on the DOF most critical to the completion of a task (Scholz and Schoner, 1999).

Understanding how the neuromuscular system controls wrist and forearm movements involving redundancy is critical to designing human-machine interfaces that reduce the risk of RSI. Knowing the origin of these forces is likewise critical if natural wrist and forearm movement is to be emulated or restored.

Despite the advances furnished by this research, several aspects could be further refined to provide more accurate results. The research presented here was all, to some degree, based off of a 3-DOF wrist and forearm model. The stiffness values used in this model were only valid for small angle movements, and had been linearized. Removing these simplifications would result in a more complete model. There also remains a great deal of potential research with the current 3-DOF model, such as modeling essential tremor in the wrist, modeling the effect of orthotics on wrist movement, and modeling the effect of tool use on the wrist.

REFERENCES

Aizawa, J., Masuda, T., Koyama, T., Nakamaru, K., Isozaki, K., Okawa, A., Morita, S., 2010. Three-dimensional motion of the upper extremity joints during various activities of daily living. J Biomech 43, 2915-2922.

Alexander, R.M., 1997. A minimum energy cost hypothesis for human arm trajectories. Biological Cybernetics 76, 97-105.

Anderton, W., Charles, S., Year Kinematic coupling of wrist and forearm movements. In Annual Meeting of the American Society of Biomechanics. Gainesville, FL.

Campolo, D., Formica, D., Guglielmelli, E., Keller, F., 2010. Kinematic analysis of the human wrist during pointing tasks. Exp Brain Res 201, 561-573.

Charles, S.K., Hogan, N., 2010. The curvature and variability of wrist and arm movements. Exp Brain Res 203, 63-73.

Charles, S.K., Hogan, N., 2011. Dynamics of wrist rotations. J Biomech 44, 614-621.

Charles, S.K., Hogan, N., 2012. Stiffness, not inertial coupling, determines path curvature of wrist motions. J Neurophysiol 107, 1230-1240.

Craig, J., 2004. Introduction to Robotics: Mechanics and Control (3rd Edition). Prentice Hall.

de Leva, P., 1996. Adjustments to Zatsiorsky-Seluyanov's segment inertia parameters. J Biomech 29, 1223-1230.

Dolan, J.M., Friedman, M.B., Nagurka, M.L., 1993. Dynamic and Loaded Impedance Components in the Maintenance of Human Arm Posture. Ieee Transactions on Systems Man and Cybernetics 23, 698-709.

Dounskaia, N., 2005. The internal model and the leading joint hypothesis: implications for control of multi-joint movements. Exp Brain Res 166, 1-16.

Gelfman, R., Melton, L.J., Yawn, B.P., Wollan, P.C., Amadio, P.C., Stevens, J.C., 2009. Long-term trends in carpal tunnel syndrome. Neurology 72, 33-41.

Gielen, C., Houk, J.C., 1984. Nonlinear Viscosity of Human Wrist. J Neurophysiol 52, 553-569.

Hill, D., 1968. Tension due to interaction between the sliding filaments in resting striated muscle. The effect of stimulation. The Journal of physiology 199, 637-684.

Hollerbach, J.M., Flash, T., 1982. Dynamic Interactions between Limb Segments During Planar Arm Movement. Biological Cybernetics 44, 67-77.

Holzbaur, K.R.S., Murray, W.M., Delp, S.L., 2005. A model of the upper extremity for simulating musculoskeletal surgery and analyzing neuromuscular control. Annals of Biomedical Engineering 33, 829-840.

Kawato, M., 1999. Internal models for motor control and trajectory planning. Curr Opin Neurobiol 9, 718-727.

Lemay, M.A., Crago, P.E., 1996. A dynamic model for simulating movements of the elbow, forearm, and wrist. J Biomech 29, 1319-1330.

Peaden, A., Charles, S.K., Dynamics of wrist and forearm rotations. In review.

Perreault, E.J., Kirsch, R.F., Crago, P.E., 2004. Multijoint dynamics and postural stability of the human arm. Exp Brain Res 157, 507-517.

Scholz, J.P., Schoner, G., 1999. The uncontrolled manifold concept: identifying control variables for a functional task. Exp Brain Res 126, 289-306.

Tsuji, T., Morasso, P.G., Goto, K., Ito, K., 1995. Human Hand Impedance Characteristics During Maintained Posture. Biological Cybernetics 72, 475-485.

van Andel, C.J., Wolterbeek, N., Doorenbosch, C.A.M., Veeger, D., Harlaar, J., 2008. Complete 3D kinematics of upper extremity functional tasks. Gait & Posture 27, 120-127.

van Tulder, M., Malmivaara, A., Koes, B., 2007. Repetitive strain injury. Lancet 369, 1815-1822.

Walker-Bone, K., Palmer, K.T., Reading, I., Coggon, D., Cooper, C., 2004. Prevalence and impact of musculoskeletal disorders of the upper limb in the general population. Arthritis & Rheumatism-Arthritis Care & Research 51, 642-651.

Wu, G., van der Helm, F.C.T., Veeger, H.E.J., Makhsous, M., Van Roy, P., Anglin, C., Nagels, J., Karduna, A.R., McQuade, K., Wang, X.G., Werner, F.W., Buchholz, B., 2005. ISB recommendation on definitions of joint coordinate systems of various joints for the reporting of human joint motion - Part II: shoulder, elbow, wrist and hand. J Biomech 38, 981-992.

APPENDIX

In order to simulate a motion with the dynamic model presented in Chapter 2.5 it may be desirable to define both a path and a velocity profile for the movement. In this model the wrist and forearm were treated as a universal joint, so the region of space that can be reached by an end effector point located on the hand is a semi-sphere with the joint origin at the center of its base. To move this end effector between any two points on this sphere a path must be defined, which here is chosen to be the arc that traverses the shortest distance possible between these two points. The coordinates system must also be configured to provide a series of points along this arc that adhere to a pre-determined velocity profile.

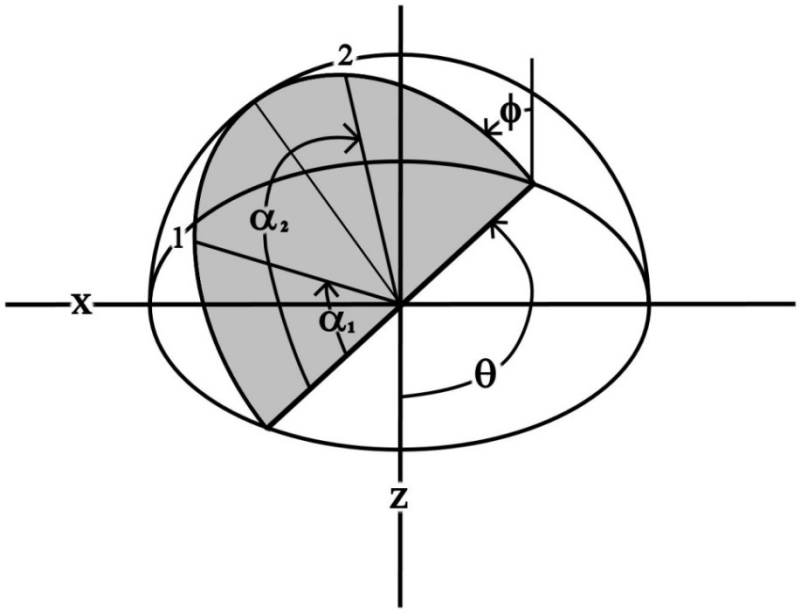

Figure A-0-1: Coordinate system for minimum distance path between two points (labeled 1 and 2) on a semi-sphere

The shortest distance path between the start and end point (points 1 and 2, Figure A-0-1) lies on the arc that is formed by the intersection of the semi-sphere of possible end-effector points and a plane that intersects the start point, end points, and origin. The velocity profile for the path between these two points is chosen by applying some function to α, the rotation angle of arc along this plane. Since the radius remains constant in this configuration, the magnitude of the velocity of the end-effector will be the tangential velocity:

$$|V| = r * |\dot{\alpha}| \quad \text{[A-1]}$$

Thus, the after the path is chosen, the velocity profile may chosen by incrementing α according to the desired function. For simplicity's sake, in this derivation the sphere is assumed to have a radius of one. The end points, if known in the coordinate system shown in Figure A-0-1, can be determined in Cartesian space as follows

$$x_1 = \sin\theta \cos\alpha_1 + \cos\theta \sin\phi \sin\alpha_1 \quad \text{[A-2]}$$

$$y_1 = \sin\alpha_1 \cos\phi \quad \text{[A-3]}$$

$$z_1 = \cos\theta \cos\alpha_1 - \sin\theta \sin\phi \sin\alpha_1 \quad \text{[A-4]}$$

The same relations can likewise be used for the second point.

Reversing this relationship to find the coordinates of the end points in this new coordinate system that are known in Cartesian space is also possible. Note that because the end points lie on a sphere, if two of the three Cartesian coordinates are known, the third can be solved for.

To solve for α, θ and ϕ we first reverse the relationship for the y-coordinate (Equation A-3), so that the values for α_1 and α_2 can be partially determined:

$$\alpha_1 = \sin^{-1}\frac{y_1}{\cos\phi}$$
$$\alpha_2 = \sin^{-1}\frac{y_2}{\cos\phi} \quad \text{[A-5]}$$

We next define the dot product between the two vectors of end-effector points in Cartesian space for future use:

$$\psi = x_1 x_2 + y_1 y_2 + z_1 z_2 \qquad \text{[A-6]}$$

The difference in the angles α_1 and α_2 is equal to that found from the dot product:

$$\alpha_1 - \alpha_2 = \cos^{-1}\psi \qquad \text{[A-7]}$$

The lone variable left in this equation, after substituting in equations A-5 and A-6 is ϕ, which can be solved for:

$$\phi = \cos^{-1}\left(\frac{\sqrt{(\psi^2 - 1)(2y_1 y_2 \psi - y_1^2 - y_2^2)}}{\psi^2 - 1}\right) \qquad \text{[A-8]}$$

With ϕ solved for, α_1 and α_2 may be determined as well. Due to the nature of negative relations in trigonometry, the solutions for α and ϕ found thus far may be incorrect. An algorithm, or good intuition, should be used at this point to determine if the correct values are α_1 or $\pi - \alpha_1$, α_2 or $\pi - \alpha_2$ and ϕ or $-\phi$. There are, in all, 8 possible combinations of answers here to choose from. Code is provided at the end of this section which may be used to correctly select the desired combination.

Once the correct values for α_1, α_2, and ϕ are known, θ may be solved for as follows:

Rearranging Equation A-2:

$$\frac{x_1 - \sin\theta\cos\alpha_1}{\sin\phi\sin\alpha_1} = \cos\theta \qquad \text{[A-9]}$$

Repeating this for the equation for x_2, then combining the two equations and rearranging:

$$x_1 \sin\alpha_2 - \sin\theta\cos\alpha_1\sin\alpha_2 = x_2\sin\alpha_1 - \sin\theta\cos\alpha_2\sin\alpha_1$$

We can now solve for θ:

$$\theta = \sin^{-1}\left(\frac{x_1\sin\alpha_2 - x_2\sin\alpha_1}{\cos\alpha_1\sin\alpha_2 - \sin\alpha_1\cos\alpha_2}\right) \qquad \text{[A-10]}$$

Code:

```
dot=x1*x2+y1*y2+z1*z2;  %Compute Dot Product
phi=acos(-sqrt((-1+dot^2)*(2*y1*dot*y2-y2^2-y1^2))/(-1+dot^2)); %Compute Phi
at1=real(asin(y1/cos(phi)));    %Compute alpha temporary 1
at2=real(asin(y2/cos(phi)));    %Compute alpha temporary 2

%Check to see which alpha is smaller.  It is assumed that the trajectory
%travels from point 1 to point 2
if at1<at2
    smaller=at1;
else
    smaller=at2;
end

if phi ~= 100 %test all 8 possibilities
    if (smaller+real(acos(dot)))<=pi/2  %This tests to see if the start and
end point are both on the same side of the hemisphere
    disp('same side');
    ttemp=real(asin((x1*sin(at2)-x2*sin(at1))/(cos(at1)*sin(at2)-
sin(at1)*cos(at2))));  %Compute a temporary theta
    xx1=sin(ttemp)*cos(at1)+cos(ttemp)*sin(phi)*sin(at1);   %Use the derived
coordinates of alpha, phi, and theta to recompute the x and z coordinates
    zz1=cos(ttemp)*cos(at1)-sin(ttemp)*sin(phi)*sin(at1);
    xx2=sin(ttemp)*cos(at2)+cos(ttemp)*sin(phi)*sin(at2);
    zz2=cos(ttemp)*cos(at2)-sin(ttemp)*sin(phi)*sin(at2);
    tdist1=abs(real(sqrt((x1-xx1)^2+(z1-zz1)^2)))+abs(real(sqrt((x2-
xx2)^2+(z2-zz2)^2)));       %Compare the x and z coordinates just computed
with the specified x and z coordinates, x1, z1, x2, and z2.  This is done by
summing the absolute value of the distances between both the start and the
end points.
    phi=-phi; %Switch the sign of phi and try this again.  Alphas are not
affected by changing sign of phi
    ttemp=real(asin((x1*sin(at2)-x2*sin(at1))/(cos(at1)*sin(at2)-
sin(at1)*cos(at2))));  %Repeat this process for the new angle values
    xx1=sin(ttemp)*cos(at1)+cos(ttemp)*sin(phi)*sin(at1);
    zz1=cos(ttemp)*cos(at1)-sin(ttemp)*sin(phi)*sin(at1);
    xx2=sin(ttemp)*cos(at2)+cos(ttemp)*sin(phi)*sin(at2);
    zz2=cos(ttemp)*cos(at2)-sin(ttemp)*sin(phi)*sin(at2);
    tdist2=abs(real(sqrt((x1-xx1)^2+(z1-zz1)^2)))+abs(real(sqrt((x2-
xx2)^2+(z2-zz2)^2)));
    at3=pi-at1;
    at4=pi-at2;
    phi=-phi;   %revert to original phi first.
    ttemp=real(asin((x1*sin(at4)-x2*sin(at3))/(cos(at3)*sin(at4)-
sin(at3)*cos(at4))));
    xx1=sin(ttemp)*cos(at3)+cos(ttemp)*sin(phi)*sin(at3);
    zz1=cos(ttemp)*cos(at3)-sin(ttemp)*sin(phi)*sin(at3);
    xx2=sin(ttemp)*cos(at4)+cos(ttemp)*sin(phi)*sin(at4);
    zz2=cos(ttemp)*cos(at4)-sin(ttemp)*sin(phi)*sin(at4);
    tdist3=abs(real(sqrt((x1-xx1)^2+(z1-zz1)^2)))+abs(real(sqrt((x2-
xx2)^2+(z2-zz2)^2)));
    phi=-phi;
    ttemp=real(asin((x1*sin(at4)-x2*sin(at3))/(cos(at3)*sin(at4)-
sin(at3)*cos(at4))));
    xx1=sin(ttemp)*cos(at3)+cos(ttemp)*sin(phi)*sin(at3);
```

```
    zz1=cos(ttemp)*cos(at3)-sin(ttemp)*sin(phi)*sin(at3);
    xx2=sin(ttemp)*cos(at4)+cos(ttemp)*sin(phi)*sin(at4);
    zz2=cos(ttemp)*cos(at4)-sin(ttemp)*sin(phi)*sin(at4);
    tdist4=abs(real(sqrt((x1-xx1)^2+(z1-zz1)^2)))+abs(real(sqrt((x2-
xx2)^2+(z2-zz2)^2)));
    phi=-phi;   %revert to original phi again.
    tvec=[tdist1 tdist2 tdist3 tdist4]; %Select the case that positions x and
z values computed from alpha1, alpha2, phi, and theta closest to the desired
values (should be only computational numeric error)
    switch min(tvec)
        case tdist1
        alpha1=at1;
        alpha2=at2;
        %Phi does not change.
        case tdist2
        alpha1=at1;
        alpha2=at2;
        phi=-phi;
        case tdist3
        alpha1=at3;
        alpha2=at4;
        %phi does not change.
        case tdist4
        alpha1=at3;
        alpha2=at4;
        phi=-phi;
    end
    if tdist2==tdist3 && tdist2==min(tvec)  % Handle redundancies in case
more than one solution matches.
        alpha1=at1;
        alpha2=at2;
        phi=-phi;
    end
    if tdist1==tdist4 && tdist1==min(tvec)
        alpha1=at1;
        alpha2=at2;
    end
    if tdist1==tdist2 && tdist1==min(tvec)
        alpha1=at1;
        alpha2=at2;
    end
    if tdist3==tdist4 && tdist3==min(tvec)
        alpha1=at3;
        alpha2=at4;
    end
    end
    if (smaller+real(acos(dot)))>pi/2   %Repeat this entire process if alpha1
and alpha2 are on opposite sides of the hemisphere
    disp('Opposite side');
    at1=pi-at1;
    ttemp=real(asin((x1*sin(at2)-x2*sin(at1))/(cos(at1)*sin(at2)-
sin(at1)*cos(at2))));
    xx1=sin(ttemp)*cos(at1)+cos(ttemp)*sin(phi)*sin(at1);
    zz1=cos(ttemp)*cos(at1)-sin(ttemp)*sin(phi)*sin(at1);
    xx2=sin(ttemp)*cos(at2)+cos(ttemp)*sin(phi)*sin(at2);
    zz2=cos(ttemp)*cos(at2)-sin(ttemp)*sin(phi)*sin(at2);
```

```
    tdist1=abs(real(sqrt((x1-xx1)^2+(z1-zz1)^2)))+abs(real(sqrt((x2-
xx2)^2+(z2-zz2)^2)));
    phi=-phi; %Alphas are not affected by changing sign of phi
    ttemp=real(asin((x1*sin(at2)-x2*sin(at1))/(cos(at1)*sin(at2)-
sin(at1)*cos(at2))));
    xx1=sin(ttemp)*cos(at1)+cos(ttemp)*sin(phi)*sin(at1);
    zz1=cos(ttemp)*cos(at1)-sin(ttemp)*sin(phi)*sin(at1);
    xx2=sin(ttemp)*cos(at2)+cos(ttemp)*sin(phi)*sin(at2);
    zz2=cos(ttemp)*cos(at2)-sin(ttemp)*sin(phi)*sin(at2);
    disp(abs(real(sqrt((x1-xx1)^2+(z1-zz1)^2))));
    disp(abs(real(sqrt((x2-xx2)^2+(z2-zz2)^2))));
    tdist2=abs(real(sqrt((x1-xx1)^2+(z1-zz1)^2)))+abs(real(sqrt((x2-
xx2)^2+(z2-zz2)^2)));
    at3=pi-at1;
    at4=pi-at2;
    phi=-phi;   %revert to original phi first.
    ttemp=real(asin((x1*sin(at4)-x2*sin(at3))/(cos(at3)*sin(at4)-
sin(at3)*cos(at4))));
    xx1=sin(ttemp)*cos(at3)+cos(ttemp)*sin(phi)*sin(at3);
    zz1=cos(ttemp)*cos(at3)-sin(ttemp)*sin(phi)*sin(at3);
    xx2=sin(ttemp)*cos(at4)+cos(ttemp)*sin(phi)*sin(at4);
    zz2=cos(ttemp)*cos(at4)-sin(ttemp)*sin(phi)*sin(at4);
    disp(abs(real(sqrt((x1-xx1)^2+(z1-zz1)^2))));
    disp(abs(real(sqrt((x2-xx2)^2+(z2-zz2)^2))));
    tdist3=abs(real(sqrt((x1-xx1)^2+(z1-zz1)^2)))+abs(real(sqrt((x2-
xx2)^2+(z2-zz2)^2)));
    phi=-phi;
    ttemp=real(asin((x1*sin(at4)-x2*sin(at3))/(cos(at3)*sin(at4)-
sin(at3)*cos(at4))));
    xx1=sin(ttemp)*cos(at3)+cos(ttemp)*sin(phi)*sin(at3);
    zz1=cos(ttemp)*cos(at3)-sin(ttemp)*sin(phi)*sin(at3);
    xx2=sin(ttemp)*cos(at4)+cos(ttemp)*sin(phi)*sin(at4);
    zz2=cos(ttemp)*cos(at4)-sin(ttemp)*sin(phi)*sin(at4);
    tdist4=abs(real(sqrt((x1-xx1)^2+(z1-zz1)^2)))+abs(real(sqrt((x2-
xx2)^2+(z2-zz2)^2)));
    phi=-phi;   %revert to original phi again.
    tvec=[tdist1 tdist2 tdist3 tdist4];
    switch min(tvec)
        case tdist1
        alpha1=at1;
        alpha2=at2;
        %Phi does not change.
        case tdist2
        alpha1=at1;
        alpha2=at2;
        phi=-phi;
        case tdist3
        alpha1=at3;
        alpha2=at4;
        %phi does not change.
        case tdist4
        alpha1=at3;
        alpha2=at4;
        phi=-phi;
    end
    if tdist2==tdist3 && tdist2==min(tvec)
        alpha1=at1;
```

```
        alpha2=at2;
        phi=-phi;
    end
    if tdist1==tdist4 && tdist1==min(tvec)
        alpha1=at1;
        alpha2=at2;
    end
    if tdist1==tdist2 && tdist1==min(tvec)
        alpha1=at1;
        alpha2=at2;
    end
    if tdist3==tdist4 && tdist3==min(tvec)
        alpha1=at3;
        alpha2=at4;
    end
    end
end

theta=real(asin((x1*sin(alpha2)-x2*sin(alpha1))/(cos(alpha1)*sin(alpha2)-
sin(alpha1)*cos(alpha2)))); % Compute Theta

if alpha2<alpha1 %Handle path direction
    temp=-1;
else
    temp=1;
end

for v=1:1:length(t)     %Step through vector of angle values, tpos, to
compute x, y, and z point at every point of time from the start point to the
end point
xp(v)=sin(theta)*cos(alpha1+temp*tpos(v))+cos(theta)*sin(phi)*sin(alpha1+temp
*tpos(v));
yp(v)=(sin(alpha1+temp*tpos(v))*cos(phi));
zp(v)=cos(theta)*cos(alpha1+temp*tpos(v))-
sin(theta)*sin(phi)*sin(alpha1+temp*tpos(v));
end
```